Institute of Visualization and Interactive Systems

University of Stuttgart
Universitätsstraße 38
D–70569 Stuttgart

Master's Thesis Nr. 3478

Thermal Imaging for Interactive Surfaces

Yomna Abdelrahman

Course of Study:	INFOTECH
Examiner:	Prof. Dr. Albrecht Schmidt
Supervisor:	M.Sc. Alireza Sahami
	M.Sc. Stefan Schneegass
	Dr. Niels Henze
Commenced:	2013-04-15
Completed:	2013-10-15
CR-Classification:	H.5.2

Dedication

This thesis is dedicated to Mom and Dad, words are just not expressive enough to thank you adequately for everything you have done for me.

Acknowledgments

I would like to gratefully acknowledge the guidance, help and motivation of my supervisors, Alireza Sahami, Niels Henz and Stefan Schneegass.

It is with immense gratitude that I acknowledge the support and help of Prof. Dr. Albrecht Schmidt.

I would like to thank the whole HCI department specially Anja Mebus for being so friendly and helpful all the time.

This work would not have been possible without the support and encouragement of my supervisor Alireza Sahami, I am really grateful for all the ideas, time and effort you have spent with me to make this topic. You are the best mentor one can ask for and Iam really honored to get to work with you.

I would like to say big thanks to my journey partners, Ghada and Mariam.

Special thanks to Mahy, for the nights we have been up together to get this thesis done.

To Dr. Eng. Mohamed, my fiancé, and my future life partner, thank you for being there and supporting me till the end of this journey.

This thesis would have remained a dream had it not been for my family; Mum Prof. Dr. Mervat AbdelFattah and Dad Prof. Dr. Ali Zohni and the best two brothers anyone can ask for Dr. Ahmed and Dr. Abdelrahman.

Last but not least, I am indebted to God for everything.

Abstract

Thermal camera operating in Far Infrared (FIR) is considered to be underexplored in fields other than security and law enforcement. Nevertheless, recently it drawn the attention of Human Computer Interaction (HCI) researchers as a new sensory system enabling novel interactive systems. They are robust to illumination changes and using it with well-known computer vision techniques, the complexity of the interaction detection is highly reduced as compared to RGB and depth cameras. FIR radiation, however, has another undiscovered characteristic that distinguishes thermal cameras from their RGB or depth counterparts, namely thermal reflection. Commonly, surfaces reflect thermal radiation differently than visual light and can become a perfect thermal mirror. In this thesis, we show that through thermal reflection, thermal cameras can sense the space beyond their direct field of view (areas besides and even behind the camera' field of view). We investigate how thermal reflection can potentially increase the interaction space of projected surfaces using camera-projection systems. We moreover discuss the reflection characteristics of common surfaces in our vicinity in both the visual and thermal radiation bands. Using a proof-of-concept prototype, we demonstrate the increased interaction space for hand-held camera-projection system. Furthermore, we depict a number of other promising application examples that can largely benefit from the thermal reflection characteristic of surfaces.

Keywords: Thermal imaging, Thermal reflection, surface interaction, hand gestures, camera-projector system

Contents

List of figures **ix**

List of tables **xi**

1 Introduction **1**
1.1 Motivation . . . 2
1.2 Goals . . . 3
1.3 Overview . . . 4

2 Background **5**
2.1 Thermal Radiation . . . 5
2.1.1 Thermal radiation modeling . . . 6
2.1.2 Thermal radiation properties . . . 9
2.2 Thermal Imaging . . . 12
2.2.1 Thermal camera and radiation properties . . . 12
2.2.2 Thermal camera operation . . . 13

3 Related Work **17**
3.1 Thermal Imaging . . . 17
3.2 Interactive Surfaces . . . 20
3.2.1 Stationary Setup . . . 20
3.2.2 Mobile Setup . . . 21

4 Heat Transfer and Thermal Reflectivity **23**
4.1 Heat Transfer . . . 24
4.2 Thermal Reflectivity . . . 25
4.2.1 Surface Roughness . . . 26

5 Algorithm **29**
5.1 Pre-processing . . . 29

5.2 Feature extraction 36
5.2.1 Heat trace detection 36
5.2.2 Hand and finger detection 38
5.2.3 Body detection 41
5.2.4 Face detection 42
5.3 Gesture Detection 43
5.3.1 On-surface gesture detection 44
5.3.2 Mid-air gesture detection 45

6 Prototype and Experiment **47**
6.1 Hardware 48
6.2 Experiment 52
6.3 Observations 52
6.4 Limiatations 54

7 Conclusion **57**
7.1 Potential Applications 59
7.2 Future Work 62

A Emissivity Table **63**

B Surface Roughness Measurement **66**

Bibliography **76**

List of Figures

1.1 Electromagnetic Spectrum [33] 1
1.2 Through thermal reflection, a thermal camera facing a surface such as brass shown on the right also observes objects besides and behind the camera. 3

2.1 Atom Energy level transformation 5
2.2 Electromagnetic Spectrum [33] 6
2.3 Intensity distribution as defined by Planck's law 8
2.4 Normalized Intensity distribution 8
2.5 Radiation parameters 9
2.6 Reflectivity vs. Emissivity [14] 11
2.7 Types of reflection [2] 11
2.8 Effect of radiating sources on the apparent temperature. . . . 13
2.9 Thermal imaging operation steps 15

3.1 BMW driver assistance [39] 19

4.1 Original vs. Expanded interaction space. 23
4.2 Interaction techniques for the direct and reflected interaction space 24
4.3 Example for heat trace 25
4.4 Thermal specular reflection. 26
4.5 Surface reflectivity in color and infrared spectrum 27

5.1 Image Pre-processing 29
5.2 Extracted frame 30
5.3 Noise filtering output. 31
5.4 Background Model 33
5.5 Thresholding [18] 34
5.6 Iterations of the thresholding algorithm [18] 35
5.7 Threshold output 35
5.8 Feature extraction 36

5.9 Heat trace detection sequence 36
5.10 Hand and Finger Detection 38
5.11 Hand and fingers detection process 38
5.12 Hand Detection 39
5.13 Haar-like features [63] 40
5.14 Body parts detection 41
5.15 Front and Profile Face detection 42
5.16 Gesture Mapping 43
5.17 Interaction space and gesture types 43
5.18 Thresholding [18] 44
5.19 Zoom in gesture detection 45
5.20 Swipe gesture 46
5.21 Hovering gesture 46

6.1 Prototype setup 47
6.2 PI160 thermal Camera dimensions [40] 48
6.3 Measurement field of the PI160 [40] 49
6.4 Dynamic Link Library (DLL) usage for feeding image data to the system 50
6.5 Behind camera interaction 51
6.6 On the surface interaction 51
6.7 Four different surfaces that can be found in the normal office environments that we tested for their thermal reflectivity. . . 52
6.8 Hand image using the PI160 and PI450 54

7.1 A thermal camera facing a TV can monitor users sitting behind the camera through thermal reflection. 60
7.2 Facing a living room table from the top an ad-hoc tabletop setup can be created. Two persons interacting while the thermal camera solely observes through thermal reflection and by observing one user through reflection and other one in the direct field of view. 61

List of Tables

4.1 Surfaces roughness 28

5.1 The β represents the number of frames and the respective time in seconds the heat trace lasts. 37

6.1 Surfaces roughness 53

- Chapter 1 -

Introduction

Imaging technology is an infinitely progressing technology which embraces various fields including digital imaging, infrared imaging, etc. This technology can be classified according to the spectrum band in which it operates. As shown in figure 2.2 the electromagnetic spectrum is divided into several bands including RGB, depth and thermal bands. The most explored band of which, is the RGB imaging, it has been employed in different applications such as robotics, medicine, security and industrial automation. HCI is considered to be one of the most interesting operation fields of visible imaging technology. Face expression, body and hand gesture recognition are utilized to act as means of interaction. Numerous computer vision techniques and libraries are available to serve the image processing of this light spectrum band.

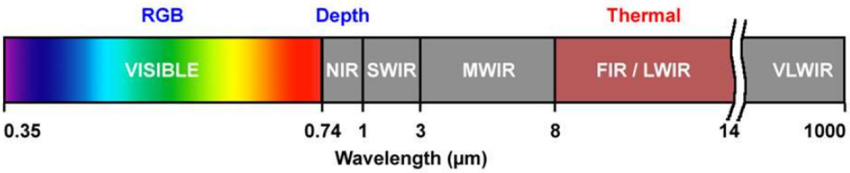

Figure 1.1: *Electromagnetic Spectrum [33]*

Unlike the RGB band, other bands especially the Thermal spectrum are not yet fully explored. The Thermal imaging technology was only limited to the military application (Surveillance systems [68]) and medical diagnostic systems (Scanning for elevated body temperature indicating swine flu). Recently, research groups have been trying to utilize its properties such as color and illumination robustness to overcome processing challenges faced in traditional RGB and depth imaging.

§ 1.1 Motivation

Thermal Imaging operating in the FIR band has shown remarkable properties, since it provides pixel-based temperature information of the objects in the field of view. It is light invariant which makes it robust to illumination changes. Moreover, easiness of segmenting heat-producing objects from the background reduces the processing complexity of object detection and segmentation. Thermal cameras are capable of sensing the thermal properties of surfaces and the human body. Such properties include heat profile of individuals, thermal reflectivity of surfaces and heat trace. This captured the attention of researches to explore and utilize this technology in more user-related fields like HCI. In order to introduce a new sensory technology enabling novel interactive systems. Thermal imaging has been recently used as a sensor for tracing users' body pose, determining emotions [44] and to recognize faces [32]. Due to their unique properties, thermal cameras have shown remarkable opportunities for interactive systems [24, 25, 33]. In these systems, a thermal camera is not only used to detect the users' position and body parts but also to trace heat trails left behind by body parts touching a surface.

RGB and depth cameras are widely used to build interactive systems by research and industry. Users can interact with such systems while they are in the camera's direct field of view. In such systems, occlusion may occur if the interaction space overlaps with the projection volume. As such cameras are sensitive to illumination or color changes, thermal cameras have been proposed as a robust alternative. A unique property of thermal cameras results from objects' varying reflection characteristics in different electromagnetic wavebands. A surface that diffuses visual light can still reflect thermal radiation. This grabs the attention to deploy thermal reflection characteristic to build interactive systems.

Additionally, the reducing cost and size of the thermal camera makes it increasingly commercially available. This makes it possible to examine and utilize thermal imaging features. Such features permit the existence of new applications for imaging technology, which were considered computationally expensive or impossible using traditional RGB imaging.

§ 1.2 Goals

In this thesis, we aim to further explore the emerging thermal imaging technology, operating in the FIR spectrum (8-14 μm). Further, investigating how to exploit surface's thermal properties to introduce a set up allowing extended interaction system. Mainly by utilizing the thermal specular[1] reflectivity of differnet surfaces acting as a mirror for the thermal camera. Thus, the camera is able to view objects in its Field of View (FOV)and visible through the surface's reflection as shown in figure 1.2. The interaction space is extended with the usage of minimal hardware (single thermal camera). It captures the mid-air gestures from the direct view as well as the reflected one and the on-surface gestures.

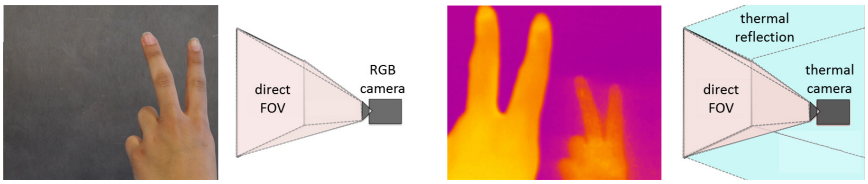

Figure 1.2: *Through thermal reflection, a thermal camera facing a surface such as brass shown on the right also observes objects besides and behind the camera.*

It is worth mentioning that, employing thermal imaging reduced the complexity of gestures detection. Moreover complement challenges faced in the RGB and depth approaches such as light dependent operation. It supports mid-air hand and body gestures as well as on-surface interactions, hence no additional devices are required (i.e. natural interaction).

In this thesis we aim to:

1. Investigation of thermal reflection and how it can be utilized to build novel interactive systems extending the interaction space beyond the field of view of the camera.
2. Implementation of a thermal camera-projection prototype as the proof-of-concept allowing users standing in front of a surface to perform hand gestures outside the thermal camera's direct field of view.
3. Analysis and assessment the reflection characteristics of different surfaces that can be found in our daily office environment .
4. Introduction and discussion of four promising application that can largely benefit from the thermal reflection phenomena.

[1] mirror like

§ 1.3 Overview

This thesis is organized as follows; Introduction which includes the introduction about imaging technology. It describes the features of thermal imaging and how we aim to utilize it to achieve the goals of the presented thesis. The background knowledge concerning this work represented in thermal radiation and thermal imaging has been thoroughly explained. Research related to the scope of this thesis is further divided into two broad sections; the first discuss the previous work using thermal imaging. The second represents the different interactive surfaces techniques. Chapter four defines the theories used including; thermal reflectivity and heat transfer. In the 'Algorithm' chapter we present the algorithms used to implement our application. Description of an interactive prototype that exploits the concept introduced is provided in chapter seven. Further, it explains the experiment carried out in order to test our system as well as presenting the observations. Finally the Conclusion and Future Work chapter describes how the presented system could be utilized in form of potential applications. Moreover, it summarizes the work presented, discusses our contribution and future work.

- Chapter 2 -

Background

This chapter provides the background knowledge concerning the technologies used throughout this thesis. It covers thermal radiation properties and how they are represented. Moreover a correlation between thermal imaging and the defined thermal properties is introduced. A brief description of how a thermal camera operates is also demonstrated.

§ 2.1 Thermal Radiation

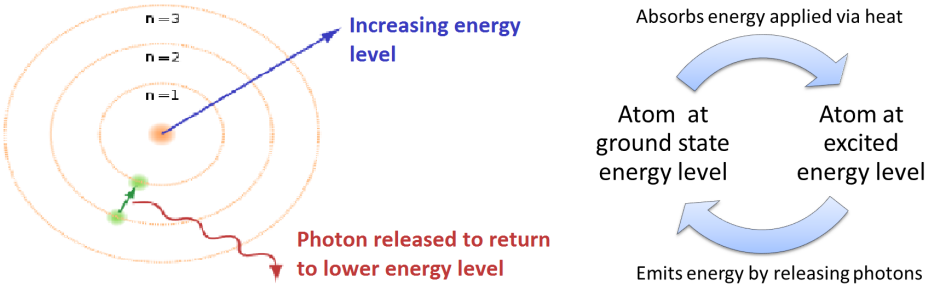

Figure 2.1: *Atom Energy level transformation*

Thermal radiation is emitted due to the object's temperature, the higher the temperature the more the object radiates. The atom consist of nucleus which itself contains proton and neutrons. This nucleus is surrounded by electron cloud in form of several orbits, which could be considered as different energy levels of the atom as presented in figure 2.1. Applying energy to an atom energy level transformation occurs due to the atom's vibration. It goes from the ground-state energy level to an excited level which is determined by the amount of the applied energy. The energy level transformation happens

due to electrons shift from lower energy orbit to higher energy orbit. As electrons travel to higher energy orbit, the atom seeks to return to its ground-state energy level. This process is achieved by releasing energy in form of photon[1].

The wavelength of the photon released is determined according to the energy state when the photon is being emitted. It is inversely proportional to the temperature of the object. That explains why when an object is being heated at the beginning no visible emission is observed. However, by reaching higher temperature it starts radiating photons with short wavelength to the extent it reaches the visible spectrum (from red and moving down within the visible spectrum).

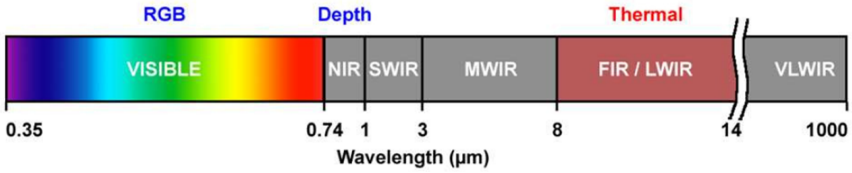

Figure 2.2: *Electromagnetic Spectrum [33]*

2.1.1 Thermal radiation modeling

The initial discovery of thermal (infrared) radiation was introduced by Sir William Herschel in 1800. He noticed increase in temperature during the assessing of the temperature of colors going down the spectrum from blue to red. Significant increase in temperature is shown as he asses the temperature of the spectrum further beyond the visible spectrum (beyond the red). From here originates the name infrared (below the red).

Thermal radiation (photons emission) is modeled by black body in thermal equilibrium. The properties of this model were defined by set of laws introduced in the 1900 by Planck, Wien, Kirchhoff, Stefan and Boltzmann. The spectrum of the emitted radiation is described by Planck's law. The frequency likelihood of the radiation is defined by Wien's displacement law. The quantity of emitted energy is given by Stefan-Boltzmann law. Each of these theoretical concepts and laws are further elaborated in detail below.

[1]elementary light particle

Black body radiation law

Black body is an ideal body that absorbs all electromagnetic radiation applied on the body's surface irrespective to the angle and frequency of the radiation. The name black body originates from the fact that it absorbs all visible electromagnetic energy and perceived as black body. It changes to red to orange to white hot when it heats up as stated by Wein Displacement Law [31]. When the black body is in thermal equilibrium state (i.e. at a constant temperature) it emits radiation according only to its temperature. The black body is as an ideal absorber (i.e. absorbs all applied radiation) and ideal emitter of radiation over all wavelength (i.e. emits the maximum energy at all wavelength). The radiation is emitted with accordance to the Planck's law as described below.

$$\alpha = \epsilon = 1 \tag{2.1}$$

Where, α :absorption
ϵ :emissivity

The Planck's law

The Planck's law defines a distribution that represents the energy level of the radiation at each wavelength (spectral specific radiation M_λ). The representation is in term of temperature T and wavelength λ.

$$M_\lambda = \frac{C_1}{\lambda^5} \frac{1}{e^{C_2/\lambda T} - 1} \tag{2.2}$$

Where, C_1 $3.74 \cdot 10^{-16}$ W m^2
C_2 $1.44 \cdot 10^{-2}$ K m

This distribution has peak values at a certain wavelength, this peak value has shorter wavelengths for higher temperatures. In other words, the wavelength of the peak of the object's radiation is inversely proportional to its absolute temperature [31]. The distribution is illustrated in figure 2.3. The concept is further elaborated in figure 2.4 by normalizing the intensity. Normalization enhances the visualization of the peak flowing to shorter wavelength at higher temperature.

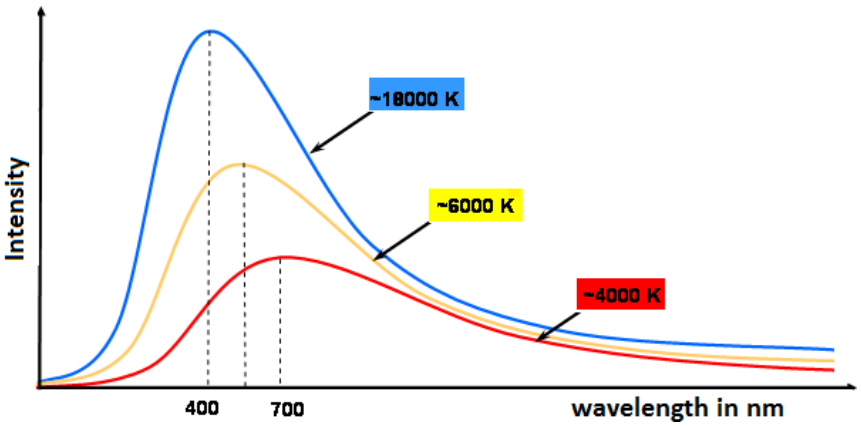

Figure 2.3: *Intensity distribution as defined by Planck's law*

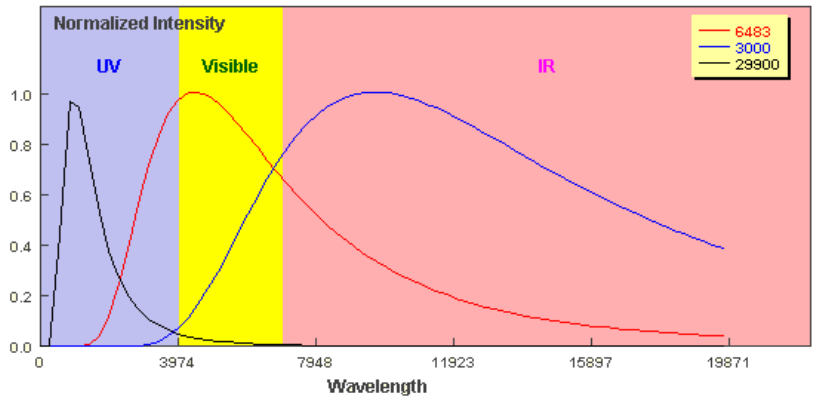

Figure 2.4: *Normalized Intensity distribution*

Wien's displacement law

As illustrated above the wavelength at the peak decreases as the temperature increases. Wien's displacement law denotes the wavelength at peak and states that it is inversely proportional to the absolute temperature. By differentiating Planck's formula a representation for Wien's displacement law could be derived as shown in equation 2.3.

$$\text{Max}\lambda = \frac{2898}{T}\mu m \cdot K \tag{2.3}$$

Stefan-Boltzmann law

Finally the Stefan-Boltzmann law defines the spectral radiation intensity at all wavelength values. By integrating the spectral radiation intensity for wavelength values the emitted radiation of the full body is computed. As shown in equation 2.4 the entire emitted radiation of a black body increases proportionally to the fourth power of its absolute temperature [31].

$$\text{Emitted radiation} \propto \text{Absolute temperature} \tag{2.4}$$

2.1.2 Thermal radiation properties

As mentioned earlier the black body is an ideal model, hence not all bodies in the real world act like the black body. Many bodies radiate less emission than the black body given the same temperature. Nevertheless Blackbody model is very useful reference to describe the radiation properties. This set of proprieties includes; emissivity, reflectivity and transmissivity [1]. The total percentage of the radiation energy could be represented by figure 5.14 and parameters equation 2.5.

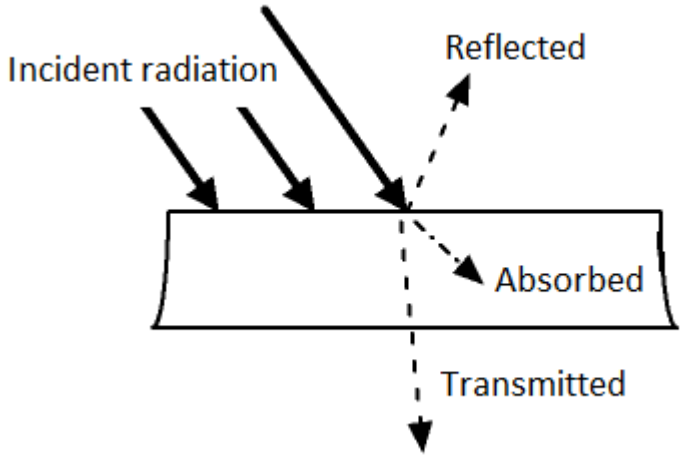

Figure 2.5: *Radiation parameters*

$$\alpha + \rho + \tau = 1 \tag{2.5}$$

Where, α : Absorption
ρ : Reflectivity
τ : Transmissivity

Absorption and Emissivity

Absorption refers to the amount of infrared energy absorbed by the body. Since the absorbed energy increase the body's temperature it is retransmitted (emitted) to reach equilibrium. Hence, we deduce the following:

$$Absorption = Emissivity \tag{2.6}$$

$$\epsilon + \rho + \tau = 1 \tag{2.7}$$

Where, ϵ : Emissivity

The emissivity values range from zero to one, since the blackbody is an ideal emitter it has emissivity value of one. This property measures the radiation ability of an object relative to that of the blackbody at the same temperature (i.e. the ability of an object to mimic the behavior of the black body).

Transmissivity

Transmissivity refers to the ability of an object to pass through thermal energy. Since, most objects cannot transmit energy this property could be ignored as presented in equation 2.8 for simplicity.

$$\epsilon + \rho = 1 \tag{2.8}$$

Reflectivity

Finally, this property is concerned with the degree of reflected energy off a body. From equation 2.8 we can deduce inversely proportional relation between the reflectivity and emissivity of an object as illustrated in figure 2.6.

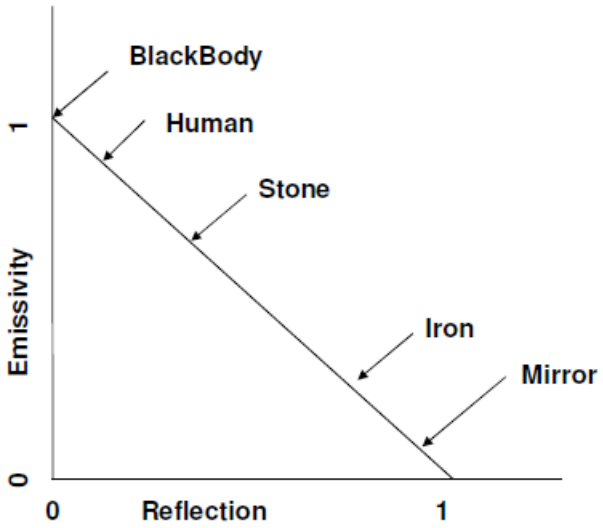

Figure 2.6: *Reflectivity vs. Emissivity [14]*

The reflectivity of an object's surface depends not only on the direction of the incident radiation but also on the direction of the reflection. Surfaces are assumed to reflect in two manners: specular and diffuse. In specular reflection, the angle of reflection equals the angle of the radiation beam. For diffuse reflection the radiation is reflected equally in all directions regardless of the incident radiation's direction. The reflectance of a surface depends on its roughness as clarified in figure 2.7 and the wavelength of radiation strikes [7].

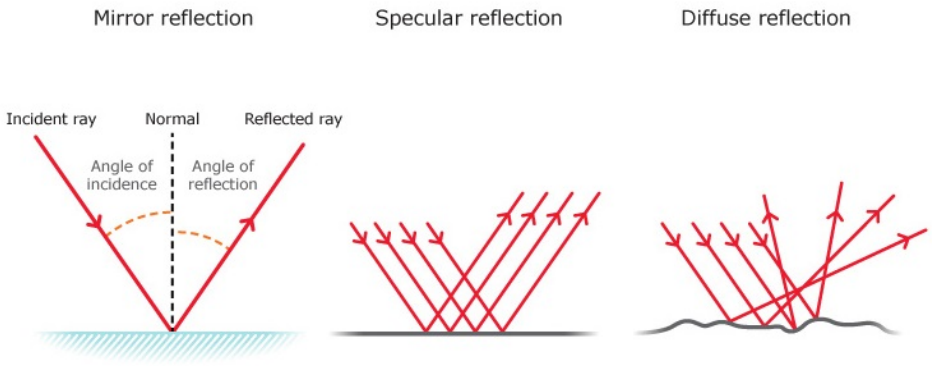

Figure 2.7: *Types of reflection [2]*

If the wavelength is smaller than the surface roughness, wave is scattered diffusely. For wavelengths much larger than the roughness dimensions, the

radiation is specularly reflected as from a mirror [53].

Beckmann & Spizzichino report that reflectance is specular if the R_a (Roughness) is smaller than one eighth (1/8) of the wavelength and otherwise diffuse [5]. The smaller the roughness is, the higher is the reflectivity. Hence, reflection from smooth and polished surfaces is mirror-like, whereas it is diffuse from rough surfaces [53].

These properties differ from one object to another depending on the object's material. Different materials exhibit different emissivity, reflectivity and transitivity proportions. For instance, plastics have an emissivity of 0.92 where aluminum has as emissivity of 0.12. Emissivity values for different object materials is listed in appendix A.

§ 2.2 Thermal Imaging

Thermal imaging is an imaging technology, in which capturing sensors are capable of passively rendering a heat map of objects in the view port. It generates an image for that heat map known as thermogram. Thermal imaging makes it possible to view the invisible heat profile of objects in the form of viewable images. This rendering is based on the thermal radiation[2] emitted by the objects only without the necessity of peripheral thermal or illumination source. This is due to the fact that thermal radiation is emitted by any object with temperature above absolute zero[3]. It is nearly impossible to have a body with temperature lower than absolute zero. Hence, thermal cameras are able to capture the heat signature of any object in its FOV.

2.2.1 Thermal camera and radiation properties

Prior explaining how thermal cameras operate, a correlation between the thermal radiation properties and what thermal cameras detect is introduced.

Emissivity and thermal camera

Thermal camera detects what is known as apparent temperature of bodies. This apparent temperature relies on both the emissivity of the body and its temperature. The real temperature of a body is not computable by thermal camera alone. If the emissivity of the body is given then the real temperature is computable by substituting the emissivity value. The emissivity and the temperature of the body both are directly proportional to the apparent

[2] Electromagnetic radiation produced by the thermal motion of charged particles in objects.

[3] 0 Kelvin, -273° Celsius and –459° Fahrenheit

temperature. Increase in one of these factors reflects an increase in the apparent temperature [1].

Reflectivity and thermal camera

In case of the existence of a radiating source, the apparent temperature detected by the thermal camera is affected. Since the camera detects the emitted and reflected radiation from the body. The apparent temperature is directly proportional to the temperature of the radiating source. In the manner that, if the radiating source has a lower temperature than the real body the apparent temperature will be lower than the real one. Correspondingly, if the radiating source has a higher temperature than the real value the apparent temperature will show higher temperature than the real temperature [1]. Figure 2.8, illustrates the effect of the radiating source on the apparent temperature computed by the thermal camera. The glass is the body of interest, where three cups of different temperature is placed as radiating source. One with same temperature as the glass (room temperature) another with higher temperature than the glass (35°C) and one with lower temperature (12°C). As revealed in figure 2.8(b) the glass apparent temperature is represented by the middle cup as it has the same temperature of the glass (it is not affecting the apparent temperature). Unlike the case of the cup of lower and higher temperature. As for the colder cup lower apparent temperature is observed and for the hotter cup higher apparent temperature is detected.

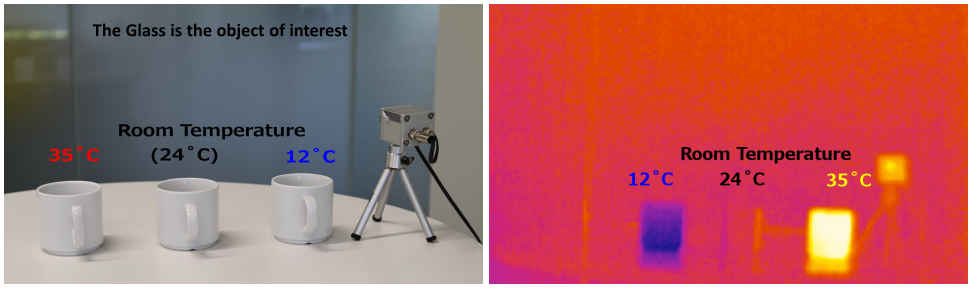

(a) *Radiating sources* **(b)** *Apparent temperature of the glass*

Figure 2.8: *Effect of radiating sources on the apparent temperature.*

2.2.2 Thermal camera operation

After defining how thermal radiation is emitted from objects and which temperature is detected by thermal cameras. This section defines how the thermal camera differs from the ordinary visible light camera and how it operates. Further, it elaborates the steps involved in mapping the object's thermal emission to thermal image for display.

Thermal cameras vs. visible light cameras

As shown in figure 2.2, the spectrum is divided into smaller bands. Each imaging systems is concerned with a specific bandwidth in which they can collect radiation. One of the main differences between thermal and visible light cameras is the spectrum of interest. Logically the visible cameras operates in the visible light spectrum whereas the thermal cameras operates in the infrared spectrum. It is worth mentioning that this infrared spectrum is further categorized into sub-bands. It includes Near Infrared (NIR), Short Wavelength Infrared (SWIR), Mid Wavelength Infrared (MWIR) and FIRwhich is also known by Long Wavelength Infrared (LWIR). The naming of these sub-bands reflects how far away they are from the center of the visible light (colors) spectrum. The main difference between the FIR/LWIR and the other infrared bands is that thermal infrared is being emitted by rather than reflected off an object. The region of interested is the FIR/LWIR spectrum since the captured thermal emission is represented by the amount of FIR/LWIR emitted by an object. This spectrum region is also called "thermal infrared" and its wavelength ranges from 8 to 14μm.

Thermal cameras perceive the emitted thermal energy form objects without the necessity of external energy source. On the other hand, the existence of light source is indispensable for the operation of visible light cameras. As visible light cameras capture the reflected visible light off the objects.

Thermal camera operation steps

As demonstrated in figure 2.9, thermal camera's lens captures the radiation emitted from objects in the view port of the camera. The collected radiation are processed by a detector to produce heat map called thermogram. The detectors used in thermal cameras utilize the Focal Plane Arrays (FPA) technology to enable the construction of 2D imaging planes. After the thermogram is created it is then transformed into electrical impulse. These impulses are further processed by signal processing unit to convert the input impulse into an image (data/information) for display. As shown in figure 2.8, various colors are presented for different emission intensity of objects [3].

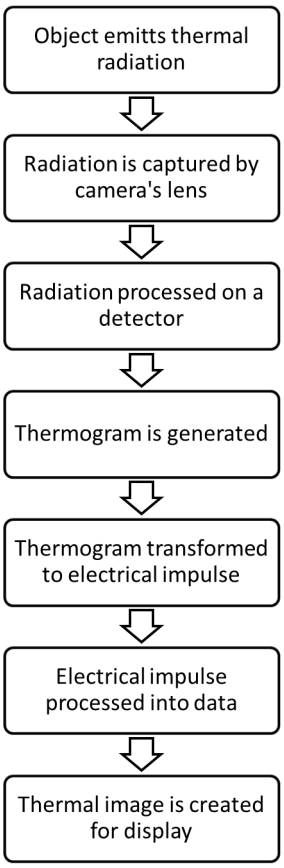

Figure 2.9: *Thermal imaging operation steps*

- Chapter 3 -

Related Work

This chapter is further divided into two broad sections. The first section represents the research and application areas of thermal imaging technology. The second section covers the different interaction setups using different imaging technologies.

§ 3.1 Thermal Imaging

Thermal imaging was first used in the late 1950s and 1960s for military applications and night vision. Researchers further developed thermal imaging techniques to be involved in other areas of applications including assisting firefighter, non-invasive quality control and medical applications [68, 42, 66]. These techniques have been further extended to be involved in more user-related applications. In this section, we will discuss how thermal imaging operates in the FIR is involved in these applications.

Surveillance Systems

Thermal imaging represented a breakthrough in the surveillance systems; since a conventional surveillance system normally needs human observers to monitor the surveillance video. This surveillance system is error prone as it depends on the degree of attention of the human observer. As thermal imaging detects the heat emitted from human body, it is able to detect the presence of humans in all lighting conditions. Moreover masking thermal contrast is not feasible making humans visible even if they are hiding in bushes or shadows. The basic concept employed for detecting humans was searching for a heat emitting object that occupies a significantly big partition of the captured image. This technique was further developed to include pattern recognition using the head position and parameter ratios [68].Such system were not only employed for anti-theft surveillance. It is also applied

in nursing home for monitoring Alzheimer patients and preventing them from leaving the nursing home without being attended to. Further, it is used for home alone faint detection system using the head detection to detect faint motion [67]. Thermal imaging illumination robustness is a major advantage. It was utilized to develop an efficient pose analysis in a crowd of people [43] to detect any irregular behavior.

It was also employed in identifying suspects by monitoring the anxiety level represented by the temperature of the individual's face [42]. This system relied on the fact that when humans are alert, anxious, or experiencing fear, their skin temperature changes. This is due to the redistributed blood flow caused by the increased adrenaline level. The periorbital, nasal, two cheeks, chin and neck area were monitored to capture any change in the temperature indicating state change.

Medical Applications

Thermal imaging has been widely applied in health research, including, for example monitoring sleep disorder. Individuals are monitored over time and the nasal area is segmented. The mean thermal profile of this region is computed and mapped to breathing information. This information is analyzed to detect sleeping disorder [29]. Further, it was utilized to gather thermal signature in the ear-skull region. Where the mobile phone is in contact with humans. This study was conducted in order to visualize and compare the associated thermal effects using different commercial mobile phones [47].

People with severe motor impairments often need a substitute access pathway. Such as a binary switch to communicate and to interact with the environment [36]. This system was based upon thermal imaging, motion tracking and morphological analysis. It detects the thermal change associated with mouth movement (opening/closing) to act as a specific binary switch.

Quality Control

The decreasing cost and size of the thermal cameras has had tremendous impact on its commercial use. For example, thermal imaging for quality control has been widely used in a diverse range of industries such as in electronic manufacturing. It was used to detect possible problems due to heat dissipation issues in circuit boards. Thermal cameras are embedded in the assembly lines, allowing non-interrupted inspection scheme. Furthermore, thermal imaging techniques have been involved in energy auditing applications. The use of thermal imaging has been extended to identify failure

points in automotive, as it is capable of capturing temperature signature at a safe distance.

Danger Spotting

BMW utilized thermal imaging in developing driver assistance systems to identify danger of collision and react accordingly. This system passively scans the environment for heat to detect the existence of humans or animals. A thermal camera is mounted in the grille to capture the temperature map of everything in front of the car. Warm objects (humans or animals) are displayed in white color, while other cooler objects (parked cars) are represented with black color. In case of the existence of pedestrian, a yellow sign appears on the display as shown in Figure 3.1. Thermal imaging allowed it to provide a heat map of a high degree of clarity at a considerable distance of 300 meters regardless of the surrounding conditions (raining, dark or existence of smoke) [39].

Figure 3.1: *BMW driver assistance [39]*

Face and expression recognition

Face recognition remains one of the most challenging tasks in computer vision. By utilizing the light independent properties of thermal imaging, a vast enhancement in the performance of face recognition can be achieved [32]. Further enhancement was found when fusing both thermal and visual imaging techniques to develop a robust illumination-invariant facial recognition [4, 20]. Thermal imaging has not only been used to recognize faces but also to classify facial expressions [29]. It has also been shown that by measuring the temperature of a user's face it is possible to determine the cognitive load and the emotional state [44].

Thermal imaging techniques were used to compute the mental load while using a computer program to evaluate the program's usability. The com-

puted mental load is gathered in order to evaluate and to enhance this computer program for better user experience. The user's cognitive load was determined by the temperature signature of the user's face. In this application, thermal cameras provide additional advantage which is a contact-less mean of information gathering.

§ 3.2 Interactive Surfaces

This section describes the previous research work in developing different interactive setups. It is categorized according to the state of the setup, either stationary or mobile interactive setup.

3.2.1 Stationary Setup

Touch and mid-air gestures are common techniques to interact with projections. These are typically detected using either RGB, infrared (IR), or depth cameras. There exists a large body of work focusing on detecting and tracking hands and fingers to enable multi-touch and mid-air gestures using RGB cameras [12, 21, 28, 35]. Such systems typically use skin color detectors [28] or template matching [21] to segment the hand and then calculate contour and convexity defects [35] to identify fingers.

Infrared imaging is a popular technique to enable multi-touch and mid-air gesture when interacting with projection screens [22, 27, 56, 58]. In such systems, the space behind the screen is typically illuminated with an infrared source and all except the infrared light is blocked from the camera using an infrared-pass filter. This technique has been widely used for tabletop interaction by combining a rear-mounted IR camera and a projection unit. Using the depth map provided by depth cameras is another approach for detecting touch and hand gestures on projected screens [38, 59, 60, 61]. These systems generally utilize either a 2D view above the surface [60, 38] or a selective 2D projection of 3D sensed data [61] for processing users input on or above the surface using common 2D computer vision techniques.

Recently, researchers explored a new field of application for the thermal imaging, such as using thermal imaging in the HCI community, including detecting and tracking user interaction on arbitrary surfaces [24, 25, 33]. This is achieved by integrating thermal imaging and existing computer vision techniques to improve user surface interaction by utilizing advantages of thermal imaging to overcome ordinary RGB and depth cameras drawbacks. Images captured from the thermal camera are light intensity independent (i.e. thermal imaging works in low- and no-light conditions, as well as good lighting and in sunlight). Daisuke and Koskue, for example, used short-lived

heat traces that result from the heat transfer from one object to another as means for interaction and created an interactive tabletop surface [24]. In such a system, a thermal camera is placed behind the surface and users can interact on the surface using warm or cold objects. The temperature map of the surface will vary allowing the detection of points of contact. Larson et al. used heat traces caused by fingers touching a surface and detected pressure for interaction on surfaces [33]. Where they trained and calibrated the heat trace using C4.5 tree classifier [48], to determine the pressure of the interaction.

Approaches to extend the interaction space beyond the surface has been investigated [62]. In such a system multiple depth cameras and projectors are deployed to allow on-surface interaction and mid-air hand gestures. However, the interaction space is still limited to areas visible by the cameras and projectors. Another technique to allow on and off the surface interaction is to place the cameras behind a transparent surface as proposed in [6, 57]. Although this setup reduces occlusion, the interaction space is limited to the FOV of the camera.

3.2.2 Mobile Setup

According to the work by Rukzio et al. [46], interaction with mobile projected displays can be divided into four categories. A common approach is to separate input and output and use the touchscreen of a mobile phone [17, 15, 50] or a touch sensor for input [8]. Sahami et al. [50] has also explored the use of the mobile phones with multi-touch surfaces as interaction means. Combined with surface interaction, tilting, throwing, and shaking of a mobile phone were translated into interaction gestures [50]. Researchers have also investigated input for mobile projection by moving and gesturing with the projector itself [8, 10, 55] or by aiming with the projector at objects in the environment [49]. Although these solutions allow users to focus on the projection and perform intuitive gestures, tracking the projector's movements requires additional hardware equipment to be installed in the room or mounted on the projector unit.

Directly touching the projection screen with the fingers [65, 19] or using a stylus [9] is another approach to interact with mobile projections. However, such a setup requires users to be very close to the projection leading to a small projection area and large shadows on the projection. Another solution is to use mid-air finger pointing and hand gestures to interact with the projection [37, 13]. Finger tracking and gesture-based interaction were introduced in [23] to allow interaction with mobile applications. The SixthSense system [37], for example, offers a set of mid-air hand gestures to support interaction with the projection. The system uses a color-based approach to

track fingers with a wearable camera. ShadowPuppets [13] provides shadow gestures as input to a hand-held projector system by casting hand shadows for co-located collaborative scenarios. Winkler et al. [64] have argued that it is more preferable to perform gestures besides or even behind the projector. This is not possible with current hand-held projectors-camera systems as both face the same direction and the projection and sensing spaces overlap. Thus, users occlude the projection while performing mid-air gestures in front of the camera.

- Chapter 4 -

Heat Transfer and Thermal Reflectivity

This chapter provides the concept and theories examined and applied in order to achieve the goal of this thesis. These concepts are utilized to expand the traditional interaction space with the minimal usage of hardware.

The work presented in this thesis, is based on utilizing thermal imaging and the thermal properties of surfaces to enlarge the interaction space. Figure 4.1 shows the original interaction space provided by traditional RGB cameras which is primarily the FOV of the camera. On the other hand, employing the thermal reflectivity of surfaces and a single thermal camera the interaction space is extended as illustrated in figure 4.1.

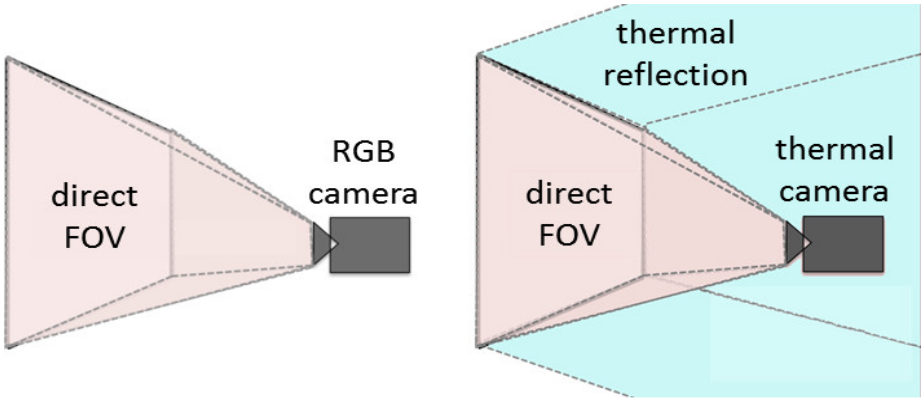

Figure 4.1: *Original vs. Expanded interaction space.*

The expanded interaction space consists of two parts, the first part is the FOV of the thermal camera. In which the interaction could be either on-surface gestures based or mid-air gestures. The second part is the additional interaction space due to thermal reflectivity of the surface. Figure 4.2, shows

the possible interaction scenarios using the direct and reflected interaction space.

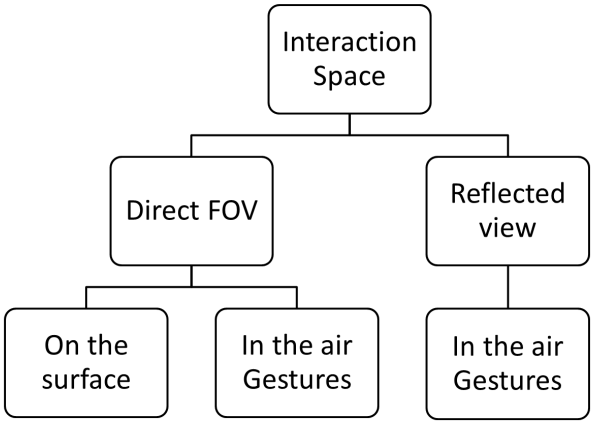

Figure 4.2: *Interaction techniques for the direct and reflected interaction space*

§ 4.1 Heat Transfer

In our system we rely on the heat transfer concept for the on-surface interaction. Principally, it states that if a warmer object in contact with a cooler surface heat transfer occurs. This transfer process causes a heat trace at the point of contact. One of the interesting features of thermal cameras is the ability to perceive heat trace. Thermal cameras capture the apparent temperature of the surface as clarified earlier in chapter 2. Heat transferred to the point of contact will show higher apparent temperature making it distinguishable in the generated image as shown in figure 5.18. In contrary, using traditional RGB and depth cameras such a trace is undetectable.

Since the temperature of the body is usually higher than the surrounding surfaces in room temperature. Touch event occurring on the surface will cause heat transfer to the point in contact, leaving heat trace behind. For instance, figure 5.18 depicts heat traces left behind due to interacting on a surface in room temperature with bare hands. Relying on this concept, interaction on arbitrary surfaces is enabled without the need of any external peripherals like gloves or special illumination conditions. This is due to the fact that the detection of the interaction is based on the invisible trace sensed by thermal camera as explained by Larson et al. [33].

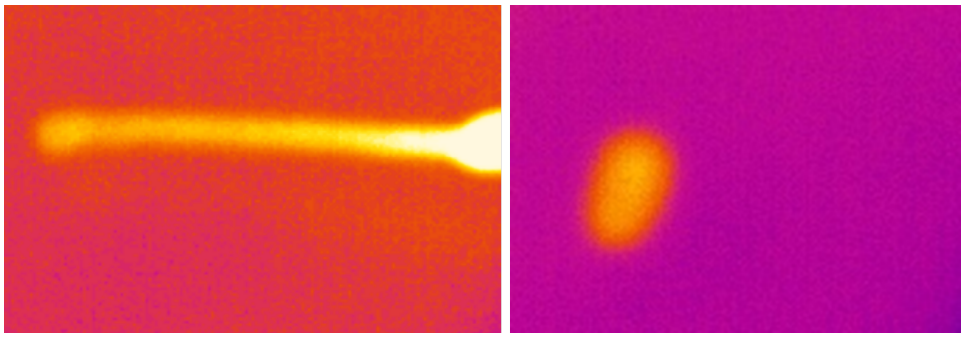

Figure 4.3: *Example for heat trace*

§ 4.2 Thermal Reflectivity

Thermal reflectivity plays a significant role in our work. Its operation and how it could be deployed to expand the interaction beyond the FOV of the camera is considered as our main research contribution. Although, it was initially assumed as a limitation and noise in other systems [33] and approaches were developed to filter them out [53].

As previously explained in section 2.1.2, thermal reflectivity refers to the amount of reflected radiation of the body surface. We exploit this property in the following manner; if a thermal camera is faced towards a surface that reflects thermal radiation in a specular way. This surface gains properties of a thermal mirror for the camera. In addition to its direct FOV, a thermal camera can thereby sense the space besides and even behind the camera through the thermal mirror.

The human body is considered as the radiating source. If the skin temperature is 33°C and the ambient temperature is 22°C it radiates waves with wavelength of 9.5 μm which lies in the FIR spectrum. On the grounds that, any surface with roughness less than one eighth of the radiation wavelength exhibits a specular reflection and the fact that the human body radiates waves with a peak wavelength of 9.5 μm. Surfaces with roughness smaller than approximately 1.18 μm (9.5/8) reflect the human radiation in specular manner. Hence, it enables the sensing of human body and hand gestures in areas that are not directly visible in the camera FOV. Figure 4.4 illustrates this surface thermal reflectivity property and human body radiating behavior. It shows both the radiating object (hand) and the specular reflected waves of the surface.

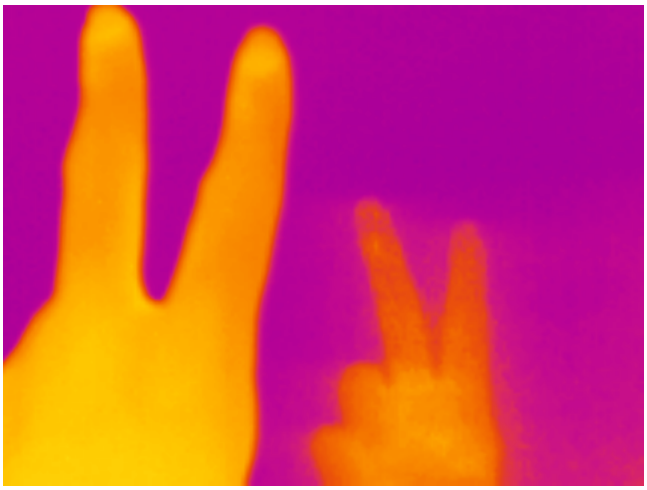

Figure 4.4: *Thermal specular reflection.*

4.2.1 Surface Roughness

Surfaces could reflect radiations either in specular or diffuse manner. Surfaces roughness correlates how surfaces reflectivity occurs. This highlights the importance of examining the roughness of various surfaces found in everyday life in order to evaluate the applicability of our proposed interaction space.

Reflectivity of surfaces differs in the visible and infrared spectrum. For instance, as clarified in figure 4.5 the surface is not reflective in the visible spectrum although it is in the FIR spectrum. This behavior difference could be utilized to allow projecting visual content but still reflect thermal radiation. As the human body radiation is in the FIR range, we are interested in surfaces that have high specular reflectivity for FIR radiation but diffuse reflectivity in the visual spectrum. Furthermore, we cannot depend on the behavior of surfaces in the color spectrum and we have to measure their roughness to specify the reflectivity in the FIR spectrum.

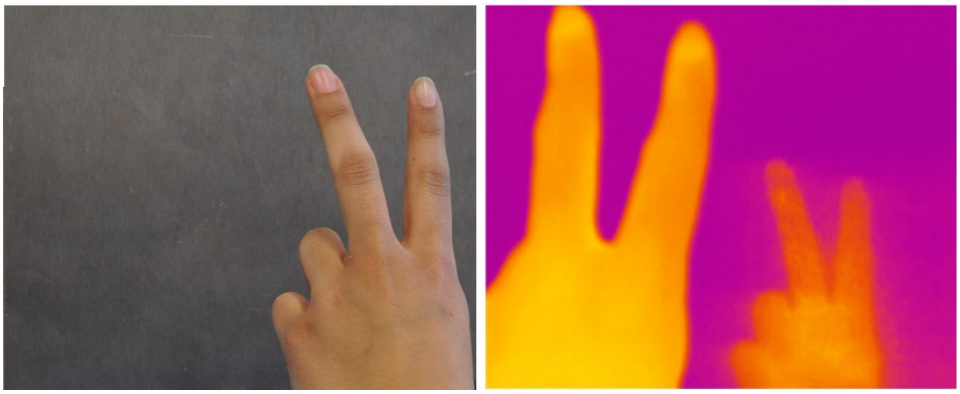

Figure 4.5: *Surface reflectivity in color and infrared spectrum*

Nine different surfaces found in the typical daily environment were picked and tested for their roughness. We measured the roughness of the surfaces used in the experiment according to ISO 4287. The topography of the surfaces were measured with a spinning micro lens confocal microscope [34, 23] (50x magnification, 0.8 numerical aperture, optical resolution below 50 nm). The roughness (Ra) was calculated with the NIST reference software[1] according to ISO 4287 from a representative slice along the measured surface. Results details could be found in appendix B

As presented in table 4.1 almost all of these surfaces have roughness lower than one eighth of the wavelength of the radiation from the human body. The glass has the smallest roughness, whereas the polished wood has the highest one. The smaller the roughness value, the more mirror-like is the surface. Painting the wood decreases its roughness by more than 90%. This opens the opportunity of adjusting the roughness of surfaces to allow specular thermal reflectivity of surfaces that originally do not exhibit such property. This proves the applicability of our proposed concepts and takes us to the next step. Which is the realization of the system that detects the gestures performed in the extended interaction space.

[1]National Institute of Standards and Technology: http://physics.nist.gov/VSC/jsp/ (last access 18.09.2013

Surface	R_a **Roughness**
Tile	0.04
Glass	0.004
Transparent Acrylic	0.005
White Acrylic	0.06
Mate Acrylic	3.49
MDF	0.11
Polished Wood	1.48
Glossy painted Polished Wood	0.11
Aluminum Plate	0.33

Table 4.1: *Surfaces roughness*

- Chapter 5 -

Algorithm

In pursuance of detecting user interaction in the extended space in form of on-surface and mid-air gestures. We have developed a system that combines thermal camera and well-known computer vision algorithms provided by Open Source Computer Vision Library (OpenCV). In this section we provide detailed explanation for the algorithms used. Throughout this section a sample hand image is used to illustrate the output of each processing step.

§ 5.1 Pre-processing

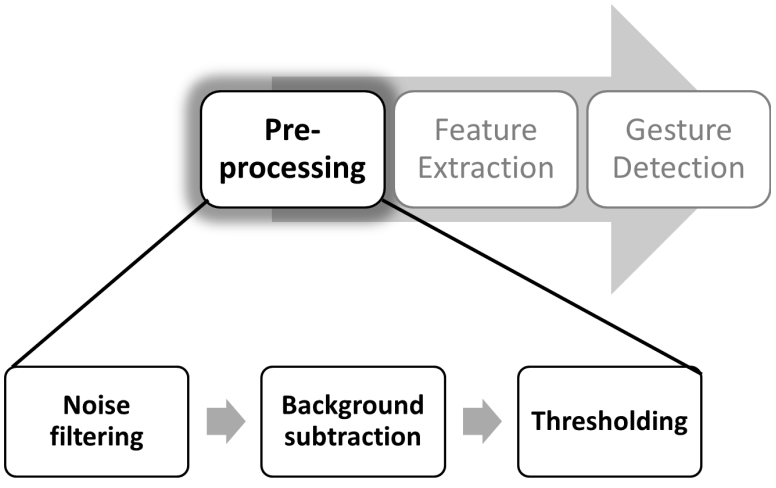

Figure 5.1: *Image Pre-processing*

The retrieved image is in the colour format as shown in figure 5.2. For each retrieved frame pre-processing is required before extracting the features. The pre-processing includes the following steps: noise filtering, background subtraction, and thresholding.

Figure 5.2: *Extracted frame*

Noise filtering

The original frame is noisy due to the hardware drift in the camera; for this reason a noise filtering is required before features extraction. In our system we applied a 5×5 pixels median filter aiming to reduce the noise.

Median Filter The operation of this filter is based on computing the pixel value according to the values of the neighboring pixels. The values in the set kernel (5×5) are rearranged and the median value of them is set to the current pixel. This makes the noise values (extreme outliers) have less effect on the pixels value, in consequence effectively removed. The fact that the pixel is dependent on the surrounding pixels (pixels representing the same feature) allows to remove the noise while preserving and not blurring the features (edges, contours,... etc.)

Since features are minimally affected by this filter we were able to apply it repeatedly. The filtering was done twice; first on the original frame. The output is converted into gray scale and the median filter is applied again. Figure 5.3 illustrates the output of the noise filtering process.

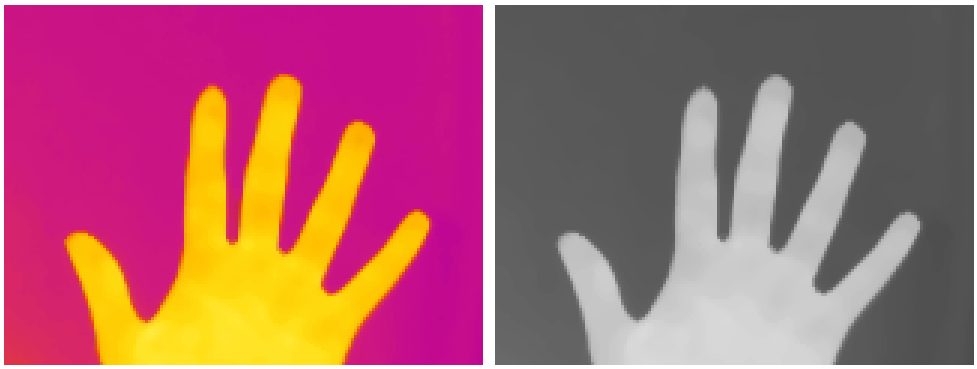

(a) *Median filter before conversion* **(b)** *Median filter after conversion*

Figure 5.3: *Noise filtering output.*

Background subtraction

The subtraction of the background is considered as one of the fundamental steps for image pre-processing. We aim to segment the foreground by computing a background model from the image sequence in order to identify regions of interest. Since our system operates in an arbitrary changing environment, a dynamic model for the background should be considered. By dynamic we refer to the ability of the model to adapt to the environment changes.

In pursuance of defining the best background modeling technique, two different dynamic algorithms were applied, tested and evaluated.

Gaussian Mixture Model as described in [69, 70] maintains a mixture of Gaussians for pixel values. For each new frame the associated mean and covariance are updated to detect any changes. In order to identify the new values as foreground or background, the Mahalanobis distance from the current value to the means is computed. If the distance is larger than a certain threshold (i.e. far enough from the mixture) it is considered as a foreground. Furthermore, this model has interesting parameters that includes the history length in which the model is updated. For instance if it set to 100, this means it will be updated every 100 frames. This considered to be very beneficial, where it is set according to the environment. Fast changing environment should has history with low values to allow faster update. On the other hand for slowly changing ones, it should be set to high value to maintain a semi-static model and save computation time.

Although this approach showed good results but it was not fast enough for our system. As our system should work in real time this model did not fit. This led us to try the second approach.

Accumulated Weighted Model computes the background as described in equation 5.1. The dynamic update is dependent on the learning rate parameter (α) that controls how fast the model is updated. The higher α, the more sensitive the background model becomes to changes in the image sequence. (i.e. as α increases, changes highly impact the computed background).

$$Model(x, y) = (1 - \alpha) \cdot Model(x, y) + \alpha \cdot Newframe(x, y) \tag{5.1}$$

The computation of this model was fairly fast and complies with our real time operation. For detecting the on surface interaction represented by the heat traces the setting of the α value is very cruical. The α value lies between zero and one and can be adjusted to either maintain heat traces until they start decaying or disappear completely.

We systematically tested the algorithm with different α values and $\alpha = 0.1$ showed the best result. Heat trace lasts in the foreground for detection yet are merged to the background fast enough to enable interaction on the same spot. Otherwise users will have to wait until the surface cools down (i.e. heat trace disappears) to touch the same spot again. The background subtraction is also essential to extract the moving interactive part (the hand) for the detection of mid-air interaction. Background subtraction step is very important as it drastically reduces false positive detection rate.

Figure 5.4, shows the model computed with different α values. As illustrated in figure 5.4a the hand is starting to be absorbed in the background, unlike figure 5.4b where it is still clear.

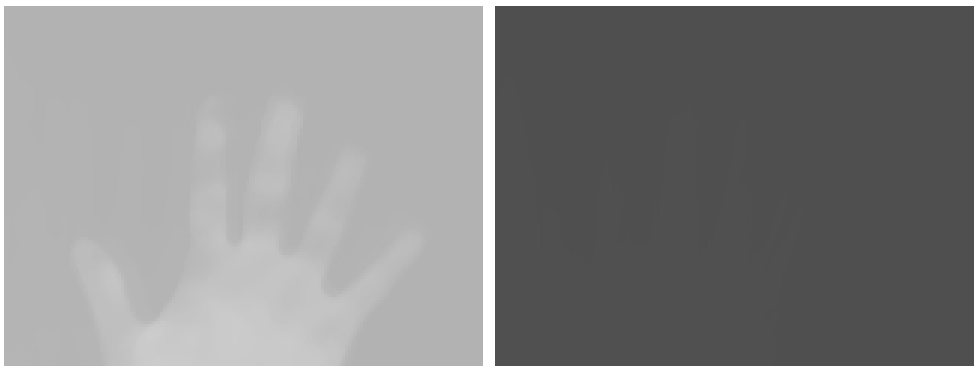

(a) α = *0.1* **(b)** α = *0.01*

Figure 5.4: *Background Model*

Thresholding

After segmenting the foreground, the final step in the pre-processing is the image binarization by thresholding. The thresholding algorithm separates parts of a human's body such as hands and fingers as well as heat traces from the rest of the foreground. We use Otsu's thresholding method [41] for identifying parts of the image that are relevant to detect body parts and heat traces.

This method assumes the existence of two classes of pixels (foreground and background). It operates in the following manner, a histogram for the gray levels in the image is created. It iterates over the gray level values to get the threshold value with minimal class overlap. The following is a simple example explaining the operation of this technique [18].

Given the following image and its corresponding histogram

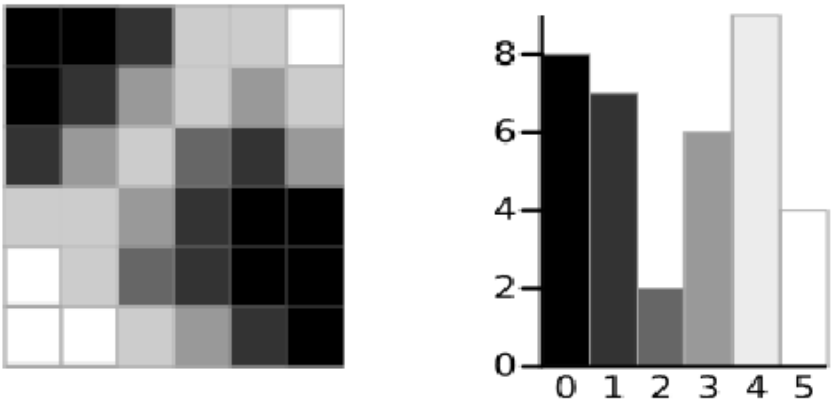

(a) *Sample 6x6 gray image* **(b)** *Histogram for gray values*

Figure 5.5: *Thresholding [18]*

The iterations carried out by the algorithm are shown below. The class overlap is represented by the within class variance. In this example threshold of value 3 shows the lowest class overlap, this makes it the best threshold value [18].

Threshold	T=0	T=1	T=2	T=3	T=4	T=5
	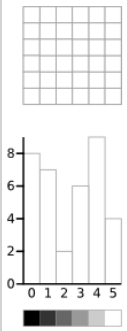	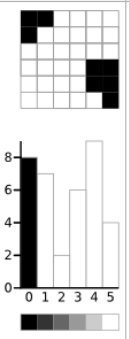	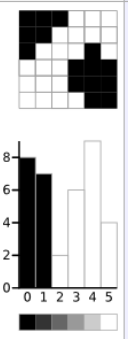	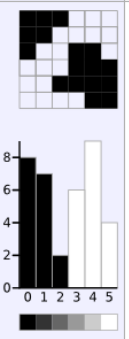	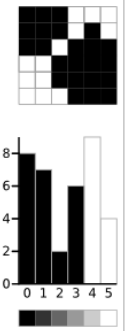	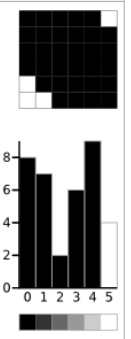
Weight, Background	W_b = 0	W_b = 0.222	W_b = 0.4167	W_b = 0.4722	W_b = 0.6389	W_b = 0.8889
Mean, Background	M_b = 0	M_b = 0	M_b = 0.4667	M_b = 0.6471	M_b = 1.2609	M_b = 2.0313
Variance, Background	σ^2_b = 0	σ^2_b = 0	σ^2_b = 0.2489	σ^2_b = 0.4637	σ^2_b = 1.4102	σ^2_b = 2.5303
Weight, Foreground	W_f = 1	W_f = 0.7778	W_f = 0.5833	W_f = 0.5278	W_f = 0.3611	W_f = 0.1111
Mean, Foreground	M_f = 2.3611	M_f = 3.0357	M_f = 3.7143	M_f = 3.8947	M_f = 4.3077	M_f = 5.000
Variance, Foreground	σ^2_f = 3.1196	σ^2_f = 1.9639	σ^2_f = 0.7755	σ^2_f = 0.5152	σ^2_f = 0.2130	σ^2_f = 0
Within Class Variance	σ^2_W = 3.1196	σ^2_W = 1.5268	σ^2_W = 0.5561	σ^2_W = 0.4909	σ^2_W = 0.9779	σ^2_W = 2.2491

Figure 5.6: *Iterations of the thresholding algorithm [18]*

Since the interactive parts stand out in the image, it separates the image into two classes (interactive part and the remaining foreground). This complies with the operation assumption of this technique.

An additional morphological closing operation is applied to enhance the boundaries of the segmented foreground and shrink the background. Figure 5.7 shows the output of this phase.

Figure 5.7: *Threshold output*

§ 5.2 Feature extraction

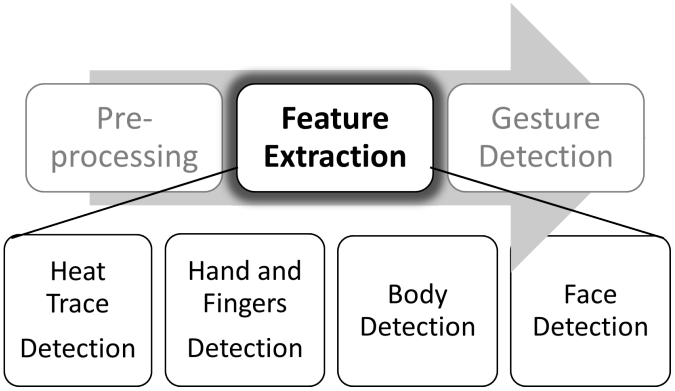

Figure 5.8: *Feature extraction*

At this point we have extracted the region of interest form the frame. Further analysis is performed to extract features and determine the type of interaction the user preforms. The interaction is either on-surface or mid-air gestures. Features of interest includes the finger tips, their relative distance and orientation for the mid-air gestures and the contours shape for the heat trace.

5.2.1 Heat trace detection

The heat transmitted from the user's hand to the surface causes the area of contact to heat up and leaves a trace. By searching for contours in the image and examining its area, shape, and temperature this trace is detected. Contours with higher temperature than the surrounding are considered as the heat trace contour. Further analysis is applied to the extracted contour to define the shape and the corresponding gesture as explained in section 5.3. Figure 5.9 summarize the entire heat trace detection process.

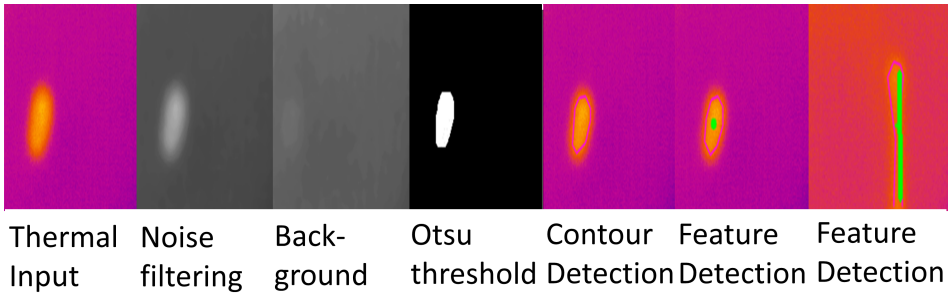

Figure 5.9: *Heat trace detection sequence*

Users may interact on the surface using different pressure levels, in our system the interaction pressure is not of importance. No calibration is required if the amount of pressure applied by the user to a surface is not important. Otherwise, the pressure can be detected through a calibration process and determining the number of frames in which the heat trace lasts (β). With two levels of pressure (high pressure and low pressure) the number of frames in which the trace persists is identified and stored. During the interaction the number of frames are compared to stored β values to deduce the pressure level of the interaction.

Surface	β **(High Pressure)**	β **(Low Pressure)**
Tile	200 (1.7 sec)	60 (0.5 sec)
Glass	220 (1.8 sec)	100 (0.8 sec)
Transparent Acrylic	170 (1.4 sec)	40 (0.3 sec)
white Acrylic	160 (1.3 sec)	44 (0.4 sec)
Mate Acrylic	250 (2.1 sec)	48 (0.4 sec)
MDF	120 (1.0 sec)	50 (0.4 sec)
Polished Wood	260 (2.2 sec)	70 (0.6 sec)
Glossy painted Polished Wood	400 (3.3 sec)	120 (1.0 sec)
Aluminum Plate	0 (0.0 sec)	0 (0.0 sec)

Table 5.1: *The β represents the number of frames and the respective time in seconds the heat trace lasts.*

This calibration is processed after noise filtering and before background subtraction. As we adjust the background subtraction learning rate (α) in such as way that we do not view old heat traces. This results in latency for detecting the pressure level. The latency depends on the camera frame rate as well as the decay rate of the heat trace on the surface. Different surface materials exhibits different decay rate, table 5.1 shows the β values of the surfaces examined in chapter 4.

5.2.2 Hand and finger detection

Hand and finger detection is considered as one of the most challenging tasks using ordinary RGB cameras. Such a task is achieved either by using skin color filter [11, 45], relying on a color map of the human skin. However, the changing skin color of different users or the lightning condition will affect the performance of such approach. Researches proposed another solution that includes using colored gloves [26, 54] to extract hand region from the images. Although this approach shows high robustness but it doesn't allow bare hand interaction (less natural).

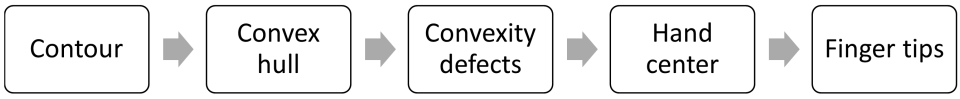

Figure 5.10: *Hand and Finger Detection*

Since the hands have a different temperature than the room temperature. They can be robustly segmented from the image in any lighting conditions using thermal imaging. As shown in figure 5.12 our algorithm computes the convex hull and convexity defects (valleys in convex hull) of the hand contour. To determine the hand center, we moreover calculate the average depth points of the defects. The finger tips are then identified as points which have local maximum distance to the computed hand center. This approach allows detecting the hand and fingers at any orientation with all possible cases (fist, open hand, 1-5 fingers).

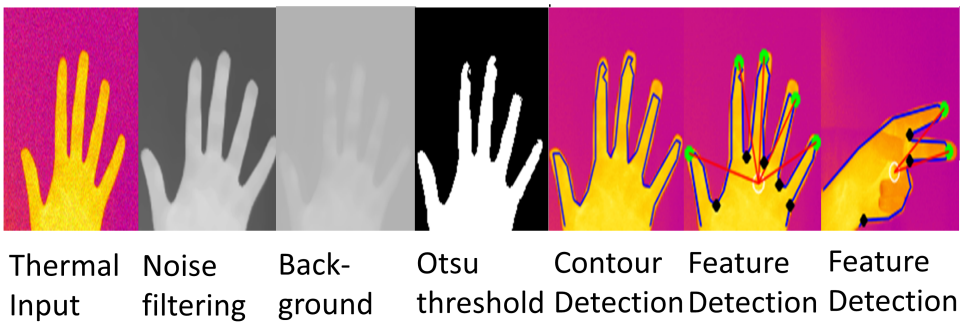

Figure 5.11: *Hand and fingers detection process*

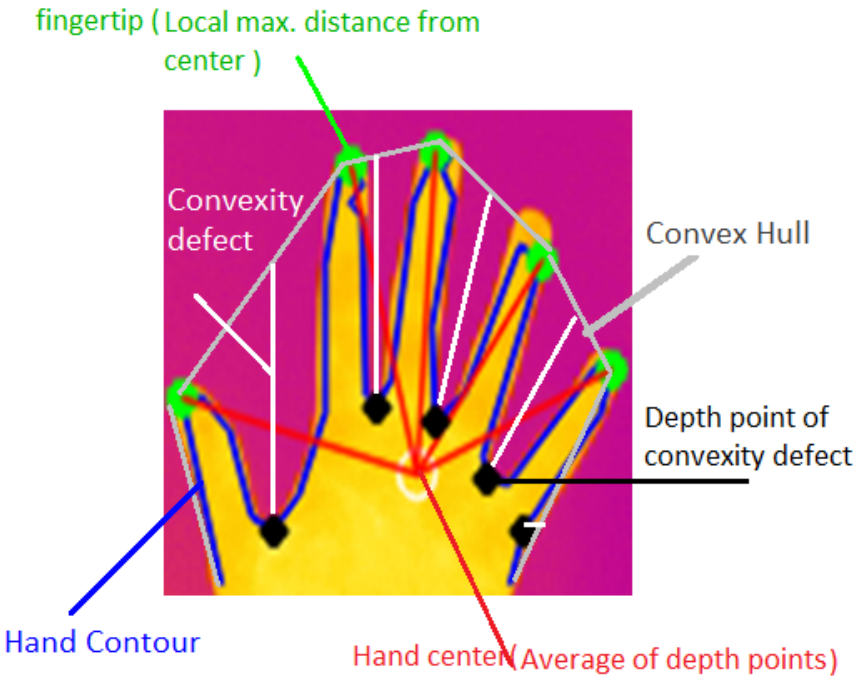

Figure 5.12: *Hand Detection*

Haar cascade classifiers

Viola and Jones [52] introduced a method to accurately detect objects using features cascade classifier. The name cascade refers to the operation manner of the classifier. The classifier is divided into stages (simpler classifier). Each stage is applied to the examined image region until it is accepted (i.e. passing all stages) or rejected. The classifier examines Haar-like features such as edges and lines as shown in figure 5.13. The classifiers for detecting body parts and face profiles have been utilized in this thesis for their detection as explained below. Further, the accuracy of the classifier detection allowed their direct usage. Hence, no new classifiers are built nor trained.

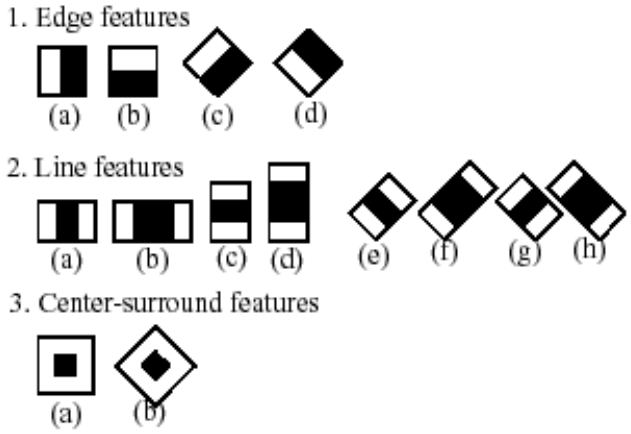

Figure 5.13: *Haar-like features [63]*

5.2.3 Body detection

Detecting the body parts introduces additional interaction technique. The detection was achieved by using full, upper and lower body classifiers provided by OpenCV. The output of the classifier is represented by set of rectangles. The results of the detection are represented by rectangles surrounding the detected part. The provided classifiers showed accurate detection. When there is no body in the image examined the set of rectangles returned was empty. The accurate detection of body parts is achieved as shown in figure 5.14.

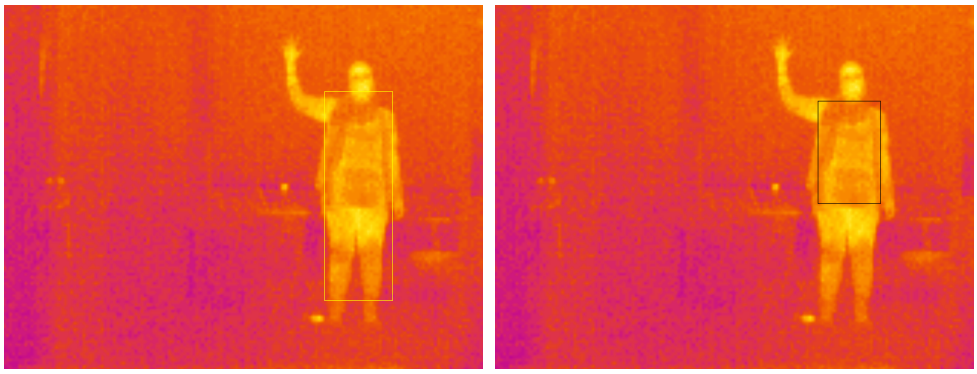

(a) *Full body* **(b)** *Upper body*

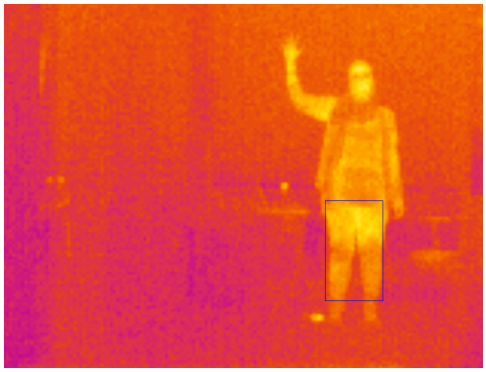

(c) *Lower body*

Figure 5.14: *Body parts detection*

5.2.4 Face detection

One of the interesting features that we could extract is the face orientation either front or profile. This was achieved by using Haar cascade classifiers [52, 34] provided by OpenCv. Since the provided classifier showed robust and accurate detection results, no special classifiers needed to be created and trained for face recognition. Tracking the extracted information could be used for matching face gestures.

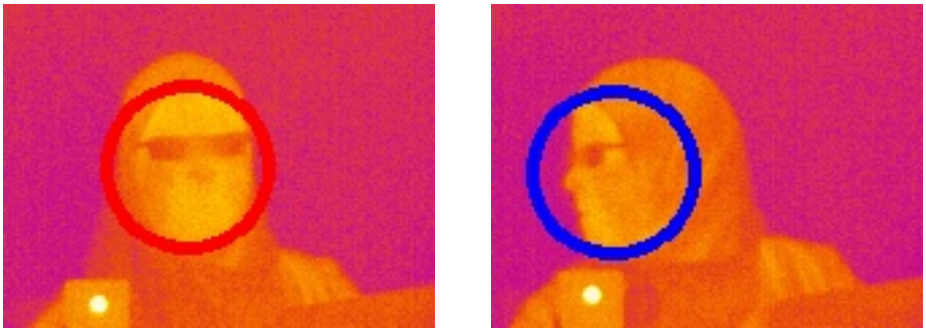

(a) *Front* **(b)** *Profile*

Figure 5.15: *Front and Profile Face detection*

§ 5.3 Gesture Detection

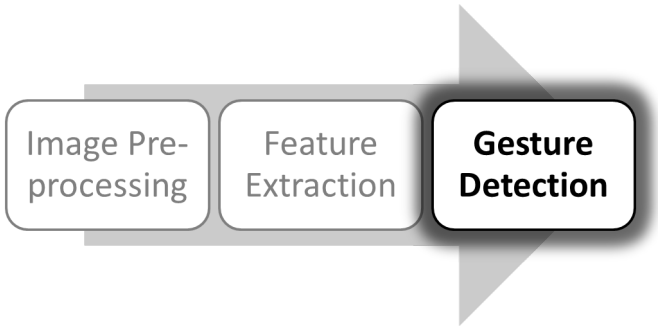

Figure 5.16: *Gesture Mapping*

After extracting the features of interest, they are used to as constraints for defining gesture and mapping them into interactive actions. Give the interaction space and types as shown in figure 5.17, an enormous gesture vocabulary could be provided. In this thesis we focused on the hand and heat trace gestures mapping. We present a set of gestures as a proof-of-concept of our proposed system.

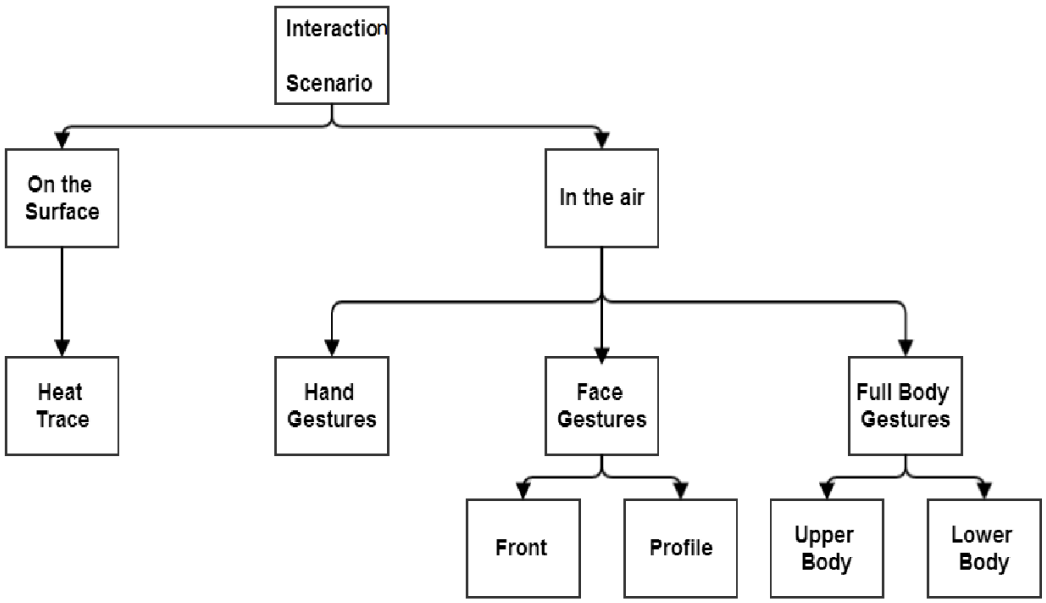

Figure 5.17: *Interaction space and gesture types*

5.3.1 On-surface gesture detection

The gesture mapping is implemented by matching the shape of the contour detected. In our system we consider two types of interaction on-surfaces, that is, touch-points or swiping in any arbitrary direction. By fitting the contour to a circle/eclipse or a line using Hough Transform [16] the interaction type is determined. The center of the contour is computed by getting the spatial moment of the extracted contour. By tracking the center of the detected line-shape contour the direction of swipe gestures is recognized. For instance, if the center is shifting to the left then it is a swipe lift. On the other hand, if a circle-shape contour is found the center is mapped into a touch point at the corresponding coordinates. Figure 5.18 shows the detection of the touch and swipe down interaction on the surface, where the green point and line representing the center and swipe respectively. Based on the heat trace, hovering and touching the surface is differentiated. Such feature is not detectable by RGB cameras.

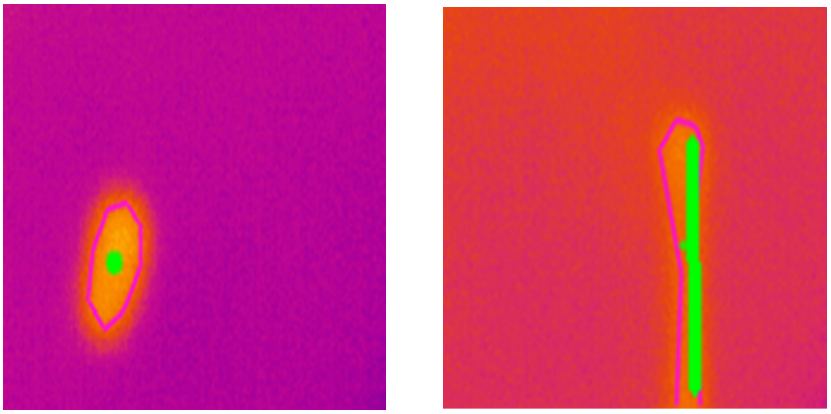

(a) *Touch heat trace* **(b)** *Swipe heat trace*

Figure 5.18: *Thresholding [18]*

5.3.2 Mid-air gesture detection

Approaches to detect hand gestures include model-based and view-based approaches. Model-based approaches utilize a 3D hand model for tracking, which makes it a complex and challenging, yet not very robust [51] task. However, view-based approaches uses the hand and finger information extracted and matches these features to patterns for hand gesture recognition. We have utilized this approach by tracking fingertips and computing their relative properties like distance, orientation... etc. to detect the following gestures:

1. **The pinch and pan gestures:**

   These gestures were used for zooming in and out by tracking the relative distance and orientation between the finger tips. If two fingertips are aligned and the distance between them is increasing then it is a zoom in. If the distance is decreasing then it is a zoom out. This approach can be used in real-time without any latency or delay. Figure 5.19a and 5.19b depicts the input from the thermal camera and the zoom in gesture detected by our system respectively.

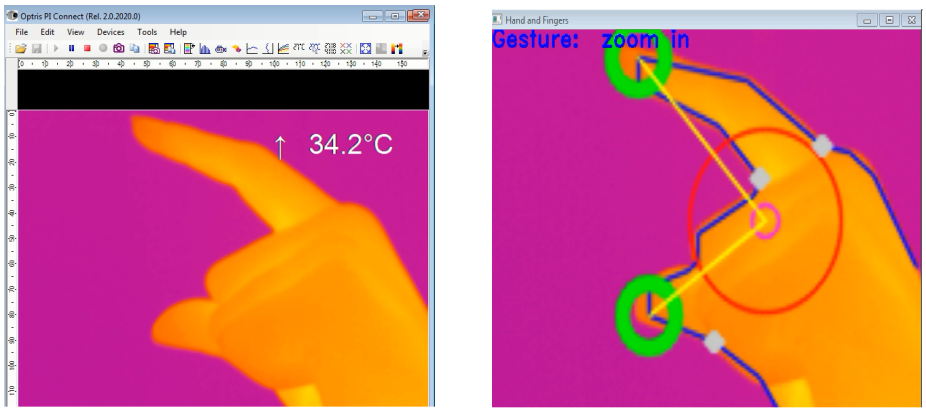

(a) *Thermal camera view* **(b)** *Gesture detection output*

Figure 5.19: *Zoom in gesture detection*

2. **In air swipe and Hovering:**

   These gestures are implemented using the finger count. If the finger count is two then it is a swipe and the fingertips are tracked to detect the swipe direction. If the finger count is one then it is a hovering gesture (i.e. no action is performed, this gesture could be used to control the mouse cursor)

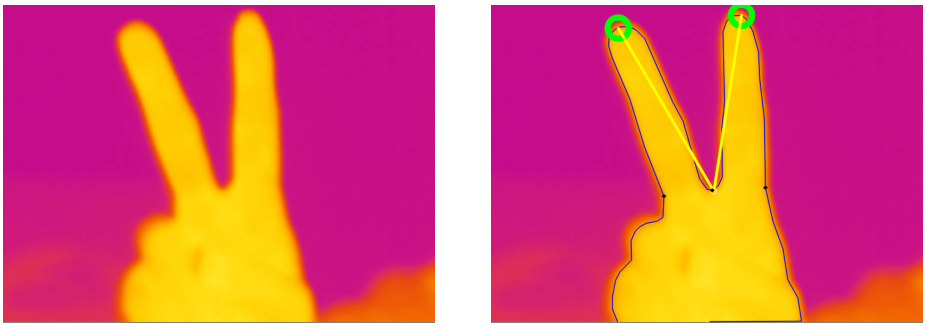

(a) *Thermal camera view* **(b)** *Gesture detection output*

Figure 5.20: *Swipe gesture*

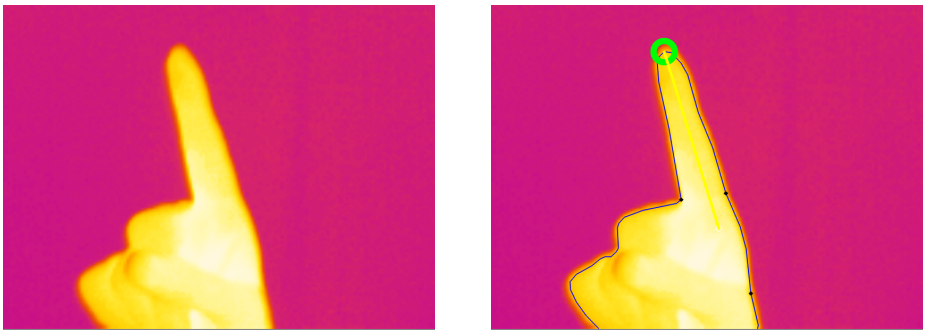

(a) *Thermal camera view* **(b)** *Gesture detection output*

Figure 5.21: *Hovering gesture*

- Chapter 6 -

Prototype and Experiment

This section describes the design of the prototype that is used as proof-of-concept to explore the concept of thermal reflectivity represented in chapter 4. The prototype runs a sample application that highlights the usage mid-air gestures and on-surface interaction using a single portable thermal camera. It further allows to have an ad-hoc mobile setup as shown in figure 6.1. It transforms surfaces with reflectivity into an interactive canvas. Moreover this prototype is used to evaluate our system performance and robustness.

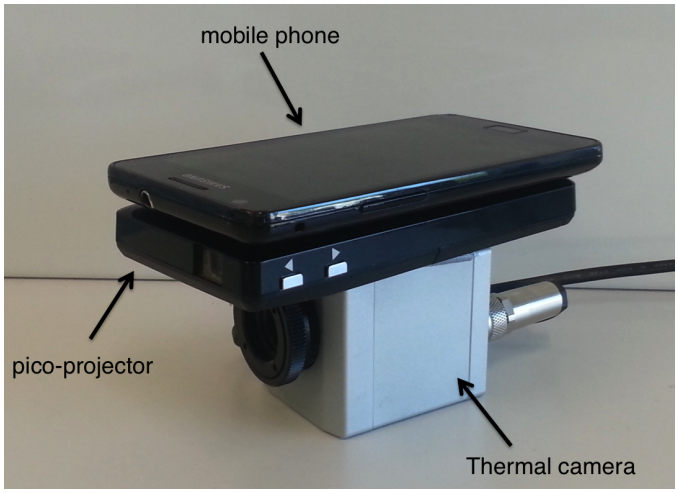

Figure 6.1: *Prototype setup*

§ 6.1 Hardware

This section describes the deployed hardware and its specification. our prototype consists of a smartphone augmented with a pico-projector[1] and a thermal camera. We used the Optris [2] PI160 thermal camera shown in figure 6.2.The camera measures and provides temperature information for the scene in a contactless and portable manner, due to its small size. The optical resolution is 160 × 120 pixels and the frame rate is 120Hz. It is able to measure the temperature range from -20°C up to 900°C with system accuracy of ±2°C. It operates with thermal sensitivity of 0.08K represented by the noise Noise Equivalent Temperature Difference (NETD) [3]. The lower the NETD the higher the sensitivity (i.e. the ability to differentiate objects in a scene with very small temperature difference between them). The wavelengths captured are in the spectral range between 7.5μm and 13μm. Interchangeable lenses are also available for the camera. The lens we used is 23° x 17° FOV [40].

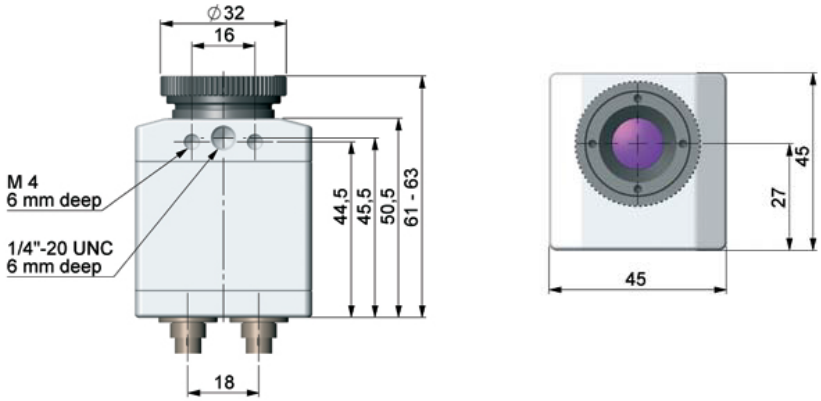

Figure 6.2: *PI160 thermal Camera dimensions [40]*

[1] MicroVision

[2] http://www.optris.com/

[3] NETD refers to the electronic noise that is interpreted as a temperature difference of an object

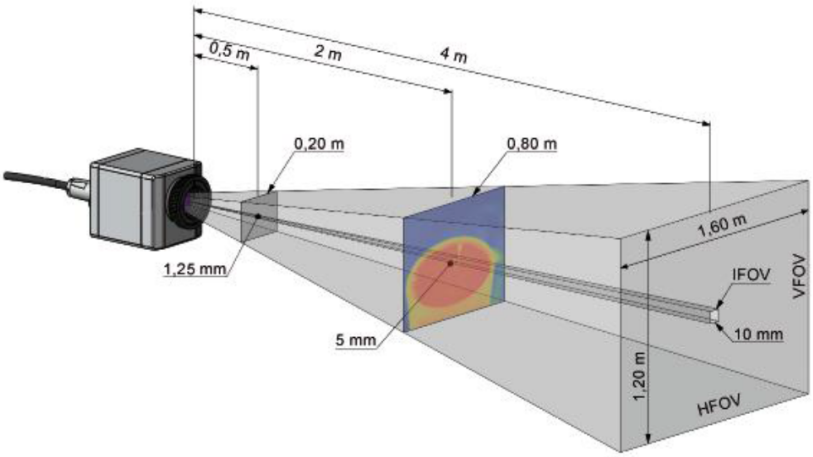

Figure 6.3: *Measurement field of the PI160 [40]*

The camera uses USB as power source as well as to transfer data. It provides raw data in one of three formats:

1. AD-Values (energy): Pixels contain pre-corrected energy values.
2. Temperature values: Pixels contain temperatures in °C.
3. YUV-colour values: YUV colour information.

We utilize the 16-bit color values. We can also compute the corresponding temperature either in one or two decimal place using the formula in 6.1 and 6.2 respectively.

$$T[^{\circ}C] = (value - 1000)/10 \tag{6.1}$$

$$T[^{\circ}C] = value/100 \tag{6.2}$$

The data is feed from the camera over USB. Unlike RGB-USB cameras where OpenCV supports the frame retrieval from the camera using built in functions. Thermal cameras is not yet supported, therefore optris provides a DLL. ImagerIPC.dll allows using the Inter Process Communication (IPC) with the Imager.exe program[4] for initiating the connection, retrieval of data as well as setting some parameters (e.g. setting the temperature range). In our implementation we dynamically link the DLL into our application. The Imager.exe external communication should be configured to IPC. Figure 6.4 illustrates the frame extraction process.

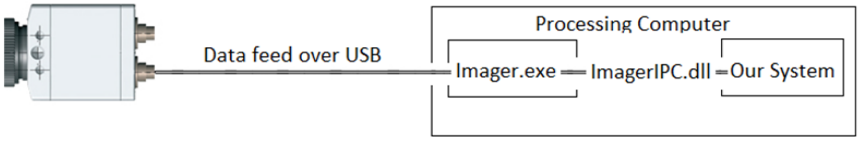

Figure 6.4: *DLL usage for feeding image data to the system*

As mentioned earlier, surfaces exhibit different reflection behavior in visible light and FIR spectrum. In our prototype we have exploited this feature to project visible content on surfaces using a pico-projector due to its diffuse reflectivity. Thermal camera is used to capture the thermal specular reflection of the surface and heat profile of the bodies in the FOV. It worth mentioning that, the projected content does not obstruct the hand and finger detection. This is due to the different operation band, where the projector emits light in the NIR and it does not reach the FIR spectrum. Hence, it is not sensed by the thermal camera and no obstruction to the hand or fingers is observed. The built prototype introduces an interactive system that can sense surface and hand gestures in front, beside and even behind a thermal camera (Optris PI160).

[4]program provided by optris to view thermal camera input

Application

OpenStreetMap application was implemented where users can pan and zoom the map information. Interaction can be either by directly touching the projection surface or by mid-air gestures. As illustrated in figure 6.5 the tile surface displays the projected visible light content yet it reflects the thermal radiation of the hand. The right figure in figure 6.5 shows the captured image by the thermal camera.

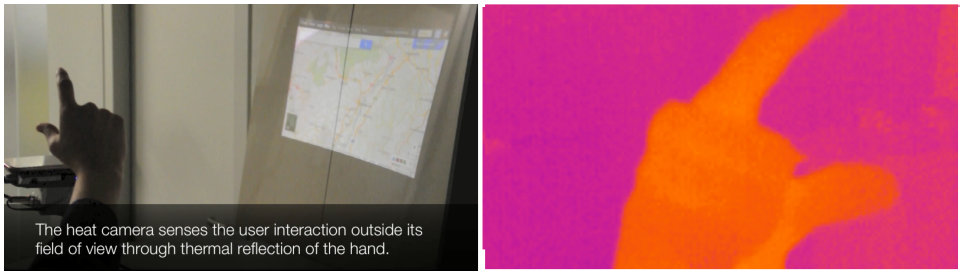

Figure 6.5: *Behind camera interaction*

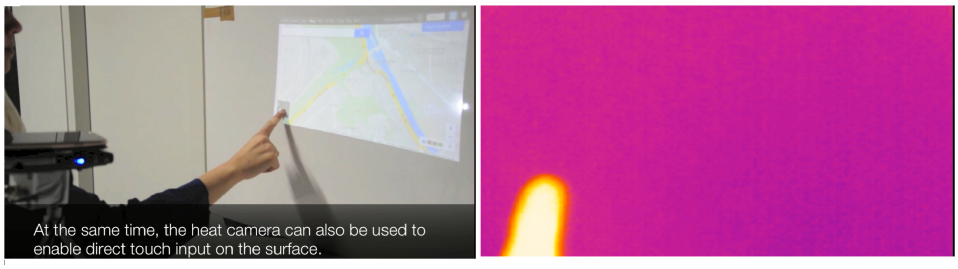

Figure 6.6: *On the surface interaction*

The prototype developed is portable. There is no constraint on the orientation, camera or projector position. Coordinates conversion is only required to map the camera coordinates to the projected coordinates. Prior interaction, the user is asked to touch the four corners of the projected view (top left, top right, bottom left and then bottom right). The center of the touch points is computed based on the center of the heat trace detected as explained before. These coordinates are the mapped to (0,0) , (159,0), (0,119) and (159,119) in order to compute the homography matrix to transform the coordinates during interaction.

§ 6.2 Experiment

Using the developed prototype an experiment was conducted to examine the robustness of our detection algorithm with four different surfaces. We focused on surfaces that can be found in normal room environment, reflect thermal radiation and can serve as a projection surface. The result of the detection algorithm is depicted in figure 6.7.

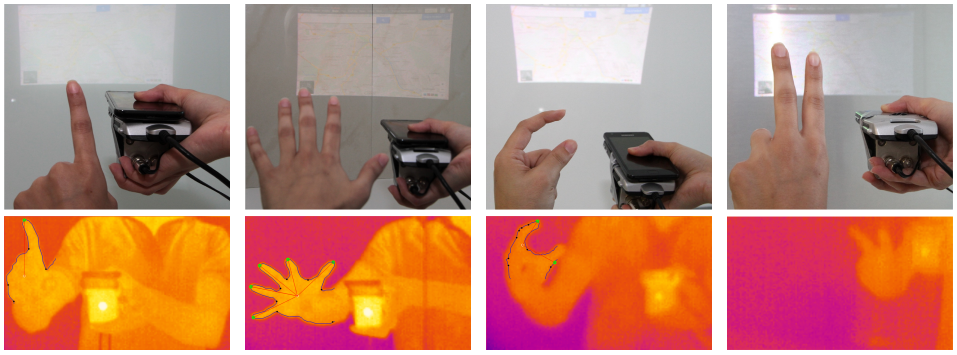

(a) *Glass* **(b)** *Tile* **(c)** *MDF* **(d)** *Aluminum*

Figure 6.7: *Four different surfaces that can be found in the normal office environments that we tested for their thermal reflectivity.*

§ 6.3 Observations

In general, shiny surfaces showed enough reflectivity to be used with our prototype. We examined the properties of the thermal reflectivity and whether it is sufficient to detect in air gestures outside of the camera's direct field of view for each of the four surfaces. For all surfaces except the polished wood and the aluminum plate, the reflectivity is high and the camera provides images with enough sharpness and contrast to detect in air gestures. Figure 6.7 shows the output images of the detection algorithm next to a visual photo of the recorded scene for four surfaces that we tested in the experiment. While glass has the highest reflectivity and tile was the second best, these two surfaces showed high detection accuracy. The MDF comes next. Finally the aluminum plate is more diffuse and provides blurry reflection which makes the detection very hard.

Surface	R_a **Roughness**
Glass	0.004
Tile	0.04
MDF	0.11
Aluminum Plate	0.33
Polished Wood	1.48
Glossy painted Polished Wood	0.11

Table 6.1: *Surfaces roughness*

Referring to the roughness values in table 6.1 and the output of the experiment in figure 6.7. We can observe the compliance of the concept that states, lower surface roughness shows higher specular thermal reflectivity.

Furthermore, one of the appealing observations is the surface thermal reflectivity behavior after painting it with glossy paint. Since the polished wood has roughness value of 1.48 no specular thermal reflectivity of the human radiation is observed, which makes it unusable for our system. However after painting it with glossy white paint its roughness was reduced to 0.11 which allows thermal specular reflectivity. From the painting experiment we can deduce that, surfaces experience lower roughness by painting them with a glossy paint. Hence, surface specular thermal reflectivity could be added or enhanced by painting it. This adds value to the proposed system, as it magnifies the set of surfaces that could be deployed with the built interaction system.

§ 6.4 Limiatations

Robust detection of hands and fingers through the processing pipeline explained above depends on the sharpness and contrast of the thermal images. In order to retrieve a sharp image the roughness of the surface should be as low as possible (e.g., smooth and polished surfaces). Surfaces with high roughness disturb the sharpness of the image rendered from the reflected heat waves, making the detection process very challenging.

The PI160 thermal camera operates with relatively low sensitivity. Other cameras such as PI450 could be used to increase the accuracy and robustness of the system, as it detects the smallest temperature difference to the extent it is capable of capturing the veins as illustrated below.

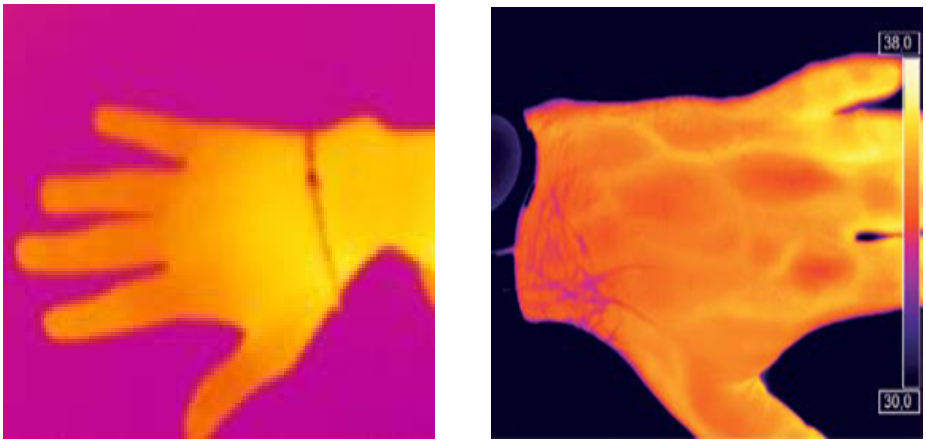

(a) *PI160* **(b)** *PI450 [40]*

Figure 6.8: *Hand image using the PI160 and PI450*

Changes in the surfaces temperature or fingertips after a long interaction session, where the surface heats up and fingers cool down, decreases the robustness of the system. Such a limitation does not apply to the in air gestures. Additionally, the heat trace is detected only when the users' finger is away from the touch point.

As described earlier, there is a latency for detecting the pressure level. This latency relays on the surface material and is directly proportional to the decay of the trace. However, the algorithms utilized to detect the interaction operate in real time especially given the resolution of the used camera (160 $\times$ 120).

In order to avoid the misinterpretation of gestures and to be able to differentiate between for example hovering over a surface and touching it. We defined a set of non-overlapping feature constraints. Heat traces were used for interaction on the surface, at least two fingertips for the in air interaction and one fingertip is detected as hovering.

- Chapter 7 -

Conclusion

In this thesis we have explored surfaces thermal reflectivity and combined it with thermal imaging technology to introduce a robust, extended and real-time interaction technique. Moreover, we illustrated how surfaces that diffuse visual light can be used as projection screen but still reflect thermal radiation.

Using such common surfaces we can extend the area observable by a thermal camera beyond its direct field of view. Relying on the fact that, surfaces exhibits specular reflectivity if its roughness is smaller than one eight of the radiated wavelength. Since we are concerned with reflection of the human body radiation (wavelength of 9.5 μm), surfaces with roughness less than 1.18 μm (9.5/8) provide specular reflectivity for human body. Hence, mid-air gestures could be detected from the reflection of the radiation. Utilizing such a setup and well-known computer vision techniques we built a camera-projector system that can monitor users gestures in front of, besides and even behind the camera. It supports on-surface gestures as well as mid-air gestures. Employing heat traces and hand/finger segemnatation for detecting the on-surface and mid-air gestures respectively. Since the capturing sensor used is a thermal camera, challenges faced using traditional RGB or depth cameras were avoided. For instance, the built system operates in illumination independent manner, where such robustness is very hard to achieve using RGB cameras.

In summary, our proposed novel interaction system provides the following advantages:

1. It can operate in any lighting condition even in dark environment as the thermal camera is illumination robust.
2. The complexity of hand and body part detection is drastically reduced as compared to RGB and depth cameras.
3. The heat trace detection enables the differentiation between hovering and touching.
4. The extended interaction space is introduced with the use of minimal hardware, where only a single thermal camera is used.
5. The projector's light does not obstruct the finger and hand detection as it emits light not in the FIR spectrum.
6. It can be easily ported and utilized in daily life since; it was tested on surfaces found in normal environment such as offices and living rooms.

An interactive prototype system was developed and used to explore the characteristics of different surfaces that could be found in the daily normal environment such as glass, tile and aluminum. We showed that a wide range of surfaces is suitable for projection and can also provide an enlarged interaction space through thermal reflection. Furthermore, we have pointed out that by painting surfaces with glossy paint their thermal reflectivity is enhanced.

Finally, four potential use cases have been examined for their applicability. It was deduced that these applications can largely benefit from the thermal reflection phenomena. Additionally, it aided the demonstration of the usability of the proposed interaction technique.

§ 7.1 Potential Applications

The developed interaction system describes the initial investigation of thermal reflectivity to extend the interaction space. We envision that thermal reflection can be used for a variety of applications. This section discusses four potential applications ideas in which thermal reflectivity can enlarge the interaction space. Consequently opens up novel possibilities for interaction in front of surfaces that reflect thermal radiation. The viability of these ideas has been assessed and found to be applicable.

Interactive (Mobile) Projection

Given the recent technological advances in manufacturing pico-projectors, we already witnessed mobile phones equipped with an embedded pico-projector. The projector extends the space for visualizing information beyond the mobile phone's display. Using current commercial systems, users interact with such systems through the phone's display. Equipping the pico-projector with a camera allows users to interact in front of the camera using mid-air gestures. Using RGB cameras in such a setup forces the user to perform the gestures in front of the camera which results in occlusion. Winkler et al. [64] already indicated that enabling users to perform gestures behind the phone might result in higher performance.

We envision that future mobile phones can be equipped with a combination of a thermal camera and a pico-projector. If the projector projects on a surface that is a mirror for the thermal camera, the camera can also observe gestures performed besides or even behind the camera and the phone. Hence, the user can perform gestures without occluding the projection.

This advantage of an increased interaction radius can not only be used for mobile projectors but also for stationary projectors. Equipping a stationary projector with a thermal camera and using a surface that reflects thermal radiation as projection screen enables to create a setup with large interactive space. The advantage is that projector and camera can be co-located which leads to a very simple setup. Users can interact directly on the surface in the camera's direct field of view as well as while being behind or besides the projector.

Interactive TVs

With the increase of inexpensive commercial sensing technologies such as depth cameras (e.g., Microsoft Kinect[1]), they have been used widely for sensing natural gesture at home. The typical setup consists of an RGB camera or a depth camera that is situated above or below the TV. Thereby the camera is looking at the living rooms. It can observe gestures performed in their direct field of view.

Figure 7.1: *A thermal camera facing a TV can monitor users sitting behind the camera through thermal reflection.*

We envision that thermal cameras to be integrated into TV's remote controllers (RC) or another mobile device and leverage thermal reflectivity once the device aims at the TV as shown in figure 7.1). This can be used in an ad-hoc scenario while holding the RC in the hand and doing bimanual interactions. For example, using the RC for activating the Electronic Program Guide (EPG) and using hand gestures for navigating through the EPG. Further, the RC can be at the living room table looking towards the TV so users can perform mid-air gestures while sitting on the sofa behind the camera.

Interactive tabletops

A typical vision-based setup to create an interactive tabletop is orienting a projector and a camera at a table that can serve as a projection screen. Camera and projector are either located above or below the surface. Each setup has its own shortcomings [58]. In a top-projection setup the user's body parts can occlude the projected image. In a rear-projection setup it becomes chalenging to capture objects that are on top of the surface or hover above. Another proposed approach is to place projector and camera at the side of the interactive surface [58]. In this setup, a difficult overhead installation of the projector is avoided. Further, the camera and projector are oblique and the occlusion problem is minimized.

[1]Microsoft Kinect - `http://www.microsoft.com/en-us/kinectforwindows/`

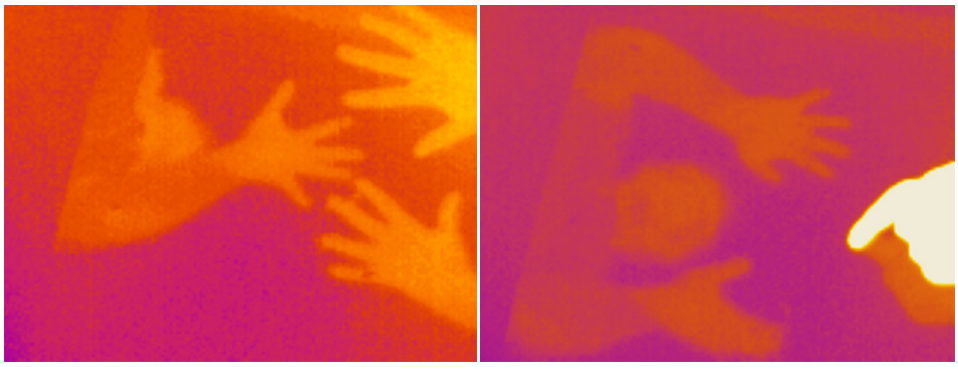

Figure 7.2: *Facing a living room table from the top an ad-hoc tabletop setup can be created. Two persons interacting while the thermal camera solely observes through thermal reflection and by observing one user through reflection and other one in the direct field of view.*

Using a thermal camera as the sensing camera together with a reflective surface can enable setups that further reduce occlusion or increase the interaction radius as illustrated in figure 7.2. When the thermal camera is oblique and the surface reflects thermal radiation, its field of view is extended. Interaction can mainly take place outside of the projection space to avoid occlusion. To have a surface that reflects human body thermal radiation, its roughness should be smaller than $1.18\mu m$. Typical tables provide this reflectivity and further surfaces can be easily created by, for example, painting a smooth wood surface glossy.

Wearable Computing

The miniaturization of computing devices has led to new types of devices that users can wear and use in various contexts (e.g., Google Glass). Interaction with such wearable devices is of great importance. Various sensors such as infrared cameras [30] have been proposed to facilitate full-body interaction. However, these sensors might be sensitive to illuminations. Further, with such camera, the user must hold the hands in the camera's direct field of view to be observable by the camera.

Considering Google Glass, for example, its RGB camera provides the opportunity to be used for observing mid-air gesture. Substituting the RGB camera with a thermal camera in front of a reflective surface, the interaction space is enlarged. Users can perform interaction behind/beside themselves out of their sight while their gestures are still visible for the camera. Furthermore, such a camera works in any light condition which is very useful for wearable devices.

§ 7.2 Future Work

This thesis presented the initial exploration of thermal imaging technology to extend the interaction space. The proposed system could be enhanced in several ways; as mentioned earlier using a more advanced camera will improve the performance, due to its higher sensitivity.

Furthermore, the set of introduced gestures could be enlarged to include face and body gestures as we already proofed their detectability using thermal camera. The hand and touch gestures set introduced is a minimal set as a proof-of-concept. However a vast vocabulary of gestures could be introduced and supported by such system. The current gesture detection system detects single had interaction. Nevertheless, it could be easily adjusted to support multiple hand interaction.

In this thesis, the viability of the suggested potential applications was proven. Nevertheless, the interactive system as well as the camera position should be adjusted to fit the proposed potential applications.

Current thermal cameras, the algorithms that have been developed for thermal imaging and the resulting systems are all optimized to reduce thermal reflection. We assume that by developing cameras, algorithms, and systems that are optimized to exploit thermal reflection we can further extend the range of surfaces that can be used for interaction through reflection. We further assume that using thermal cameras beyond the niche applications where they are currently used can bring down their cost dramatically.

- Appendix A -

Emissivity Table

Material		typical Emissivity
Asbestos		0,95
Asphalt		0,95
Basalt		0,7
Carbon	non oxidized	0,8-0,9
	graphite	0,7-0,8
Carborundum		0,9
Ceramic		0,95
Concrete		0,95
Glass		0,85
Grit		0,95
Gypsum		0,8-0,95
Ice		0,98
Limestone		0,98
Paint	non alkaline	0,9-0,95
Paper	any color	0,95
Plastic $>50\,\mu m$	non transparent	0,95
Rubber		0,95
Sand		0,9
Snow		0,9
Soil		0,9-0,98
Textiles		0,95
Water		0,93
Wood	natural	0,9-0,95

Material		typical Emissivity
Aluminium	non oxidized	0,02-0,1
	polished	0,02-0,1
	roughened	0,1-0,3
	oxidized	0,2-0,4
Brass	polished	0,01-0,05
	roughened	0,3
	oxidized	0,5
Copper	polished	0,03
	roughened	0,05-0,1
	oxidized	0,4-0,8
Chrome		0,02-0,2
Gold		0,01-0,1
Haynes	alloy	0,3-0,8
Inconel	electro polished	0,15
	sandblast	0,3-0,6
	oxidized	0,7-0,95
Iron	non oxidized	0,05-0,2
	rusted	0,5-0,7
	oxidized	0,5-0,9
	forged, blunt	0,9
Iron, casted	non oxidized	0,2
	oxidized	0,6-0,95
Lead	polished	0,05-0,1

Material		typical Emissivity
Lead	roughened	0,4
	oxidized	0,2-0,6
Magnesium		0,02-0,1
Mercury		0,05-0,15
Molybdenum	non oxidized	0,1
	oxidized	0,2-0,6
Monel (Ni-Cu)		0,1-0,14
Nickel	electrolytic	0,05-0,15
	oxidized	0,2-0,5
Platinum	black	0,9
Silver		0,02
Steel	polished plate	0,1
	rustless	0,1-0,8
	heavy plate	0,4-0,6
	cold-rolled	0,7-0,9
	oxidized	0,7-0,9
Tin	non oxidized	0,05
Titanium	polished	0,05-0,2
	oxidized	0,5-0,6
Wolfram	polished	0,03-0,1
Zinc	polished	0,02
	oxidized	0,1

Figure A.1: *Surface Emissivity [40]*

- Appendix B -

Surface Roughness Measurement

Messprotokoll **eosMetrology**
TGU, TTI GmbH

Probe	Alu weniger raue Unterseite
Datum/Zeit	05.09.2013
Messsystem	Konfokales Mikroskop mit rotierender Mikrolinsenscheibe
Messobjektiv	50x NA 0.8 Feldgröße [µm] 444,6 x 327,1
Messbereich lateral	[µm] 15700 x 327,1; Verwendung eines charakteristischen Linienschnitts
Sensorrauschen	95% innerhalb von 47 nm PV
Kalibrierung an Tiefeneinstellnormal	
Geometriekorrektur	Tiefpass (1x2), Schwellwertkriterium
Datenauswertung	Geometriekorrektur über Ausgleichsgerade, λ_C-Filter 0,8 mm über NIST-Referenzsoftware (http://physics.nist.gov/VSC/jsp/FileOpen.jsp)
Hinweise	-
Bearbeiter	Dipl. Ing. Wolfram Lyda, Dipl. Ing. David Fleischle
Ergebnisse	R_a = 0,33107 µm, R_z = 2.27587µm W_a = 0.15064 µm, W_z = 0.27988µm

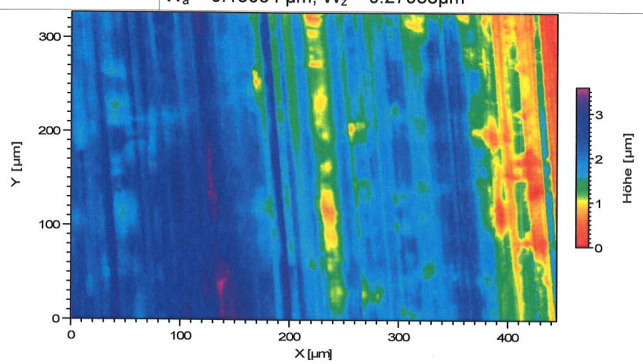

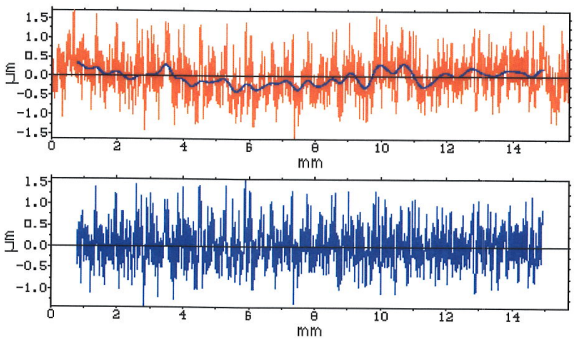

Unterschrift Sachbearbeiter

Messprotokoll

eosMetrology
TGU, TTI GmbH

Probe	Alu raue Oberseite
Datum/Zeit	05.09.2013
Messsystem	Konfokales Mikroskop mit rotierender Mikrolinsenscheibe
Messobjektiv	50x NA 0.8 Feldgröße [µm] 444,6 x 327,1
Messbereich lateral	[µm] 15700 x 327,1; Verwendung eines charakteristischen Linienschnitts
Sensorrauschen	95% innerhalb von 69 nm PV
Kalibrierung an Tiefeneinstellnormal	7,333 µm (-2,4 %), 23,58 µm (-1,9%), 73,68 µm (-1,8%)
Geometriekorrektur	Tiefpass (1x2), Schwellwertkriterium, ungültige Pixel interpoliert und ersetzt
Datenauswertung	Geometriekorrektur über Ausgleichsgerade, λ_C-Filter 0,8 mm über NIST-Referenzsoftware (http://physics.nist.gov/VSC/jsp/FileOpen.jsp)
Hinweise	Die Probenoberfläche besitzt eine transparente Lackschicht, ca. 10µm oberhalb des Aluminiums, welche die Messung beeinflusst
Bearbeiter	Dipl. Ing. Wolfram Lyda, Dipl. Ing. David Fleischle
Ergebnisse	R_a = 0.98796 µm, R_z = 5.64792 µm W_a = 0.78905 µm, W_z = 1.88995 µm

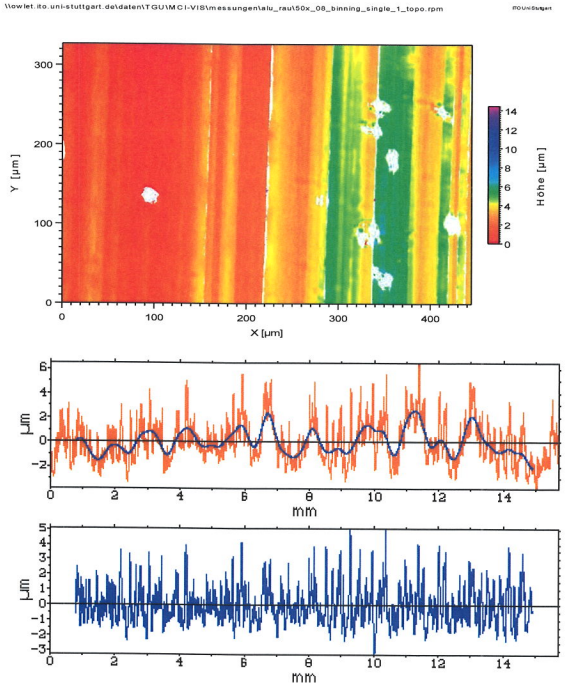

Unterschrift Sachbearbeiter

Messprotokoll

eosMetrology
TGU, TTI GmbH

Probe	Glasplatte – transparente Seite
Datum/Zeit	06.09.2013
Messsystem	Konfokales Mikroskop mit rotierender Mikrolinsenscheibe
Messobjektiv	50x NA 0.8 Feldgröße [µm] 444,6 x 327,1
Messbereich lateral	[µm] 13100 x 327,1; Verwendung eines charakteristischen Linienschnitts
Sensorrauschen	95% innerhalb von 43 nm PV
Kalibrierung an Tiefeneinstellnormal	7,333 µm (-2,4 %), 23,58 µm (-1,9%), 73,68 µm (-1,8%)
Geometriekorrektur	Tiefpass (1x2), Schwellwertkriterium, ungültige Pixel interpoliert und ersetzt
Datenauswertung	Geometriekorrektur über Ausgleichsgerade, λ_C-Filter 0,8 mm über NIST-Referenzsoftware (http://physics.nist.gov/VSC/jsp/FileOpen.jsp)
Hinweise	
Bearbeiter	Dipl. Ing. Wolfram Lyda, Dipl. Ing. David Fleischle
Ergebnisse	R_a = 0.00439 µm, R_z = 0.03999 µm W_a = 0.04436 µm, W_z = 0.0213 µm

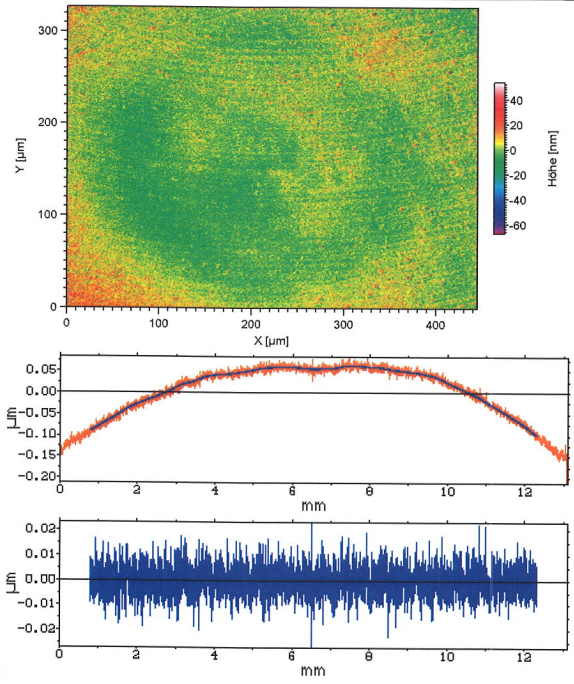

Unterschrift Sachbearbeiter

Messprotokoll

eosMetrology
TGU, TTI GmbH

Probe	Holzstück – Dick – weiße Seite
Datum/Zeit	04.09.2013
Messsystem	Konfokales Mikroskop mit rotierender Mikrolinsenscheibe
Messobjektiv	50x NA 0.8 Feldgröße [µm] 444,6 x 327,1
Messbereich lateral	[µm] 13100 x 327,1; Verwendung eines charakteristischen Linienschnitts
Sensorrauschen	95% innerhalb von 42 nm PV
Kalibrierung an Tiefeneinstellnormal	7,333 µm (-2,4 %), 23,58 µm (-1,9%), 73,68 µm (-1,8%)
Geometriekorrektur	Tiefpass (1x2), Schwellwertkriterium
Datenauswertung	Geometriekorrektur über Ausgleichsgerade, λ_C-Filter 0,8 mm über NIST-Referenzsoftware (http://physics.nist.gov/VSC/jsp/FileOpen.jsp)
Hinweise	Die Probenoberfläche zeigte eine geringe Transparenz bei 780 nm Beleuchtungswellenlänge.
Bearbeiter	Dipl. Ing. Wolfram Lyda, Dipl. Ing. David Fleischle
Ergebnisse	R_a = 0.11441 µm, R_z = 0.623 µm W_a = 0.38553 µm, W_z = 0.45065 µm

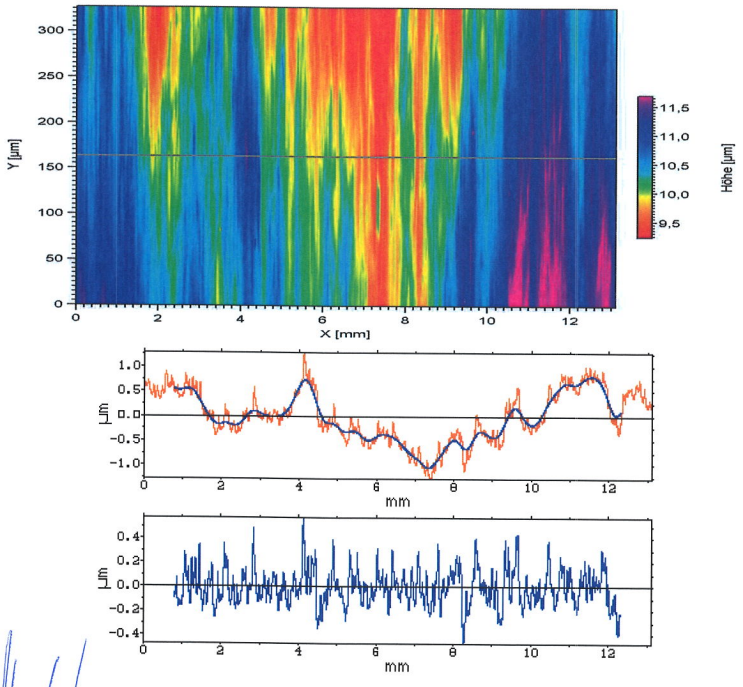

Unterschrift Sachbearbeiter

Messprotokoll

eosMetrology
TGU, TTI GmbH

Probe	Holzstück – Dünn – lackierte Seite
Datum/Zeit	04.09.2013
Messsystem	Konfokales Mikroskop mit rotierender Mikrolinsenscheibe
Messobjektiv	50x NA 0.8 Feldgröße [µm] 444,6 x 327,1
Messbereich lateral	[µm] 13100 x 327,1; Verwendung eines charakteristischen Linienschnitts
Sensorrauschen	95% innerhalb von 63 nm PV
Kalibrierung an Tiefeneinstellnormal	7,333 µm (-2,4 %), 23,58 µm (-1,9%), 73,68 µm (-1,8%)
Geometriekorrektur	Tiefpass (1x2), Schwellwertkriterium
Datenauswertung	Geometriekorrektur über Ausgleichsgerade, λ_C-Filter 0,8 mm über NIST-Referenzsoftware (http://physics.nist.gov/VSC/jsp/FileOpen.jsp)
Hinweise	-
Bearbeiter	Dipl. Ing. Wolfram Lyda, Dipl. Ing. David Fleischle
Ergebnisse	R_a = 0.11454 µm, R_z = 0.62858 µm W_a = 3.0954 µm, W_z = 3.36369 µm

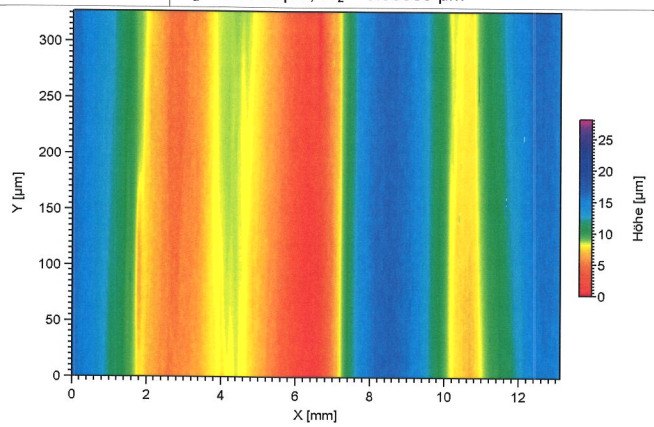

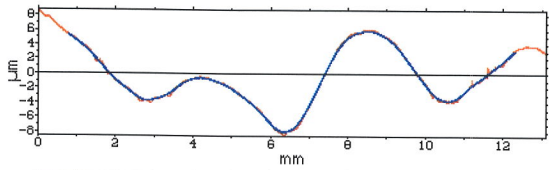

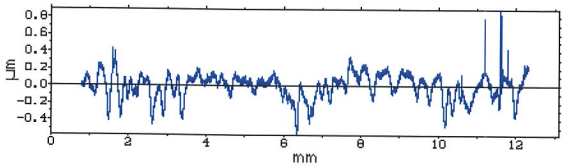

Unterschrift Sachbearbeiter

Messprotokoll

eosMetrology
TGU, TTI GmbH

Probe	Holzstück – Dünn – untere Seite
Datum/Zeit	04.09.2013
Messsystem	Konfokales Mikroskop mit rotierender Mikrolinsenscheibe
Messobjektiv	50x NA 0.8 Feldgröße [µm] 444,6 x 327,1
Messbereich lateral	[µm] 13100 x 327,1; Verwendung eines charakteristischen Linienschnitts
Sensorrauschen	95% innerhalb von 193 nm PV, Sa = 18 nm
Kalibrierung an Tiefeneinstellnormal	7,333 µm (-2,4 %), 23,58 µm (-1,9%), 73,68 µm (-1,8%)
Geometriekorrektur	Tiefpass (1x2), Schwellwertkriterium
Datenauswertung	Geometriekorrektur über Ausgleichsgerade, λ_C-Filter 0,8 mm über, λ_s-Filter 2,5µm, NIST-Referenzsoftware (http://physics.nist.gov/VSC/jsp/FileOpen.jsp)
Hinweise	-
Bearbeiter	Dipl. Ing. Wolfram Lyda, Dipl. Ing. David Fleischle
Ergebnisse	R_a = 1.48057 µm, R_z = 11.48359 µm W_a = 0.92021 µm, W_z = 1.72414 µm

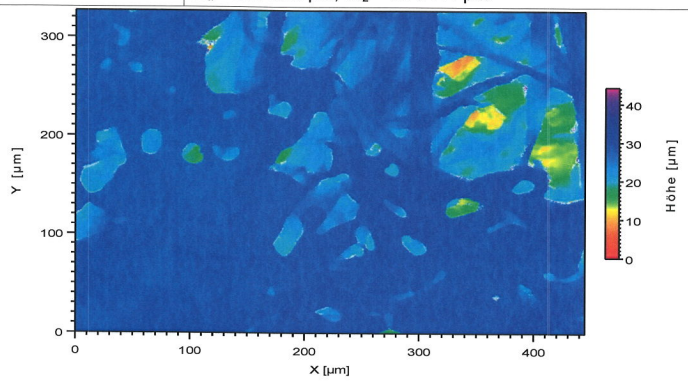

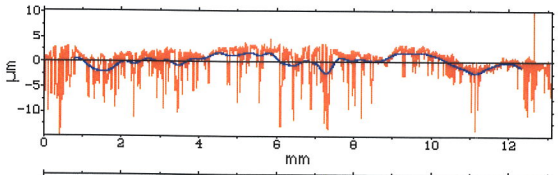

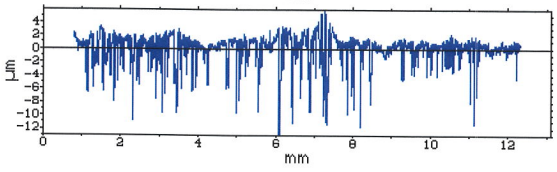

Unterschrift Sachbearbeiter

Messprotokoll

eosMetrology
TGU, TTI GmbH

Probe	Plexiglass – matte Oberfläche
Datum/Zeit	06.09.2013
Messsystem	Konfokales Mikroskop mit rotierender Mikrolinsenscheibe
Messobjektiv	50x NA 0.8 Feldgröße [µm] 444,6 x 327,1
Messbereich lateral	[µm] 15700 x 327,1; Verwendung eines charakteristischen Linienschnitts
Sensorrauschen	95% innerhalb von 265 nm PV, 29 nm RMS
Kalibrierung an Tiefeneinstellnormal	7,333 µm (-2,4 %), 23,58 µm (-1,9%), 73,68 µm (-1,8%)
Geometriekorrektur	Tiefpass (1x2), Schwellwertkriterium, ungültige Pixel interpoliert und ersetzt
Datenauswertung	Geometriekorrektur über Ausgleichsgerade, λ_C-Filter 2,5 mm über NIST-Referenzsoftware (http://physics.nist.gov/VSC/jsp/FileOpen.jsp)
Hinweise	
Bearbeiter	Dipl. Ing. Wolfram Lyda, Dipl. Ing. David Fleischle
Ergebnisse	R_a = 3.49086 µm, R_z = 25.49181 µm W_a = 0.35466 µm, W_z = 1.03976 µm

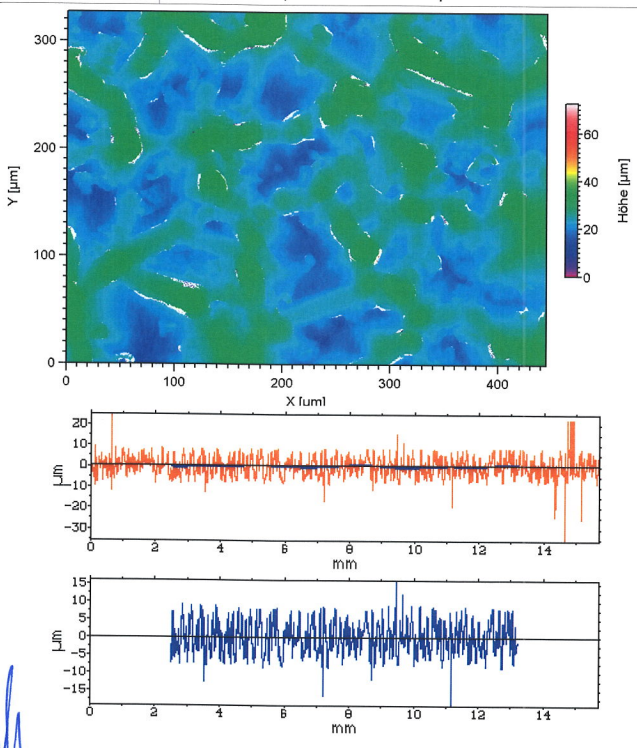

Unterschrift Sachbearbeiter

Messprotokoll

eosMetrology
TGU, TTI GmbH

Probe	Plexiglass – Milchglass
Datum/Zeit	08.09.2013
Messsystem	Konfokales Mikroskop mit rotierender Mikrolinsenscheibe
Messobjektiv	50x NA 0.8 Feldgröße [µm] 444,6 x 327,1
Messbereich lateral	[µm] 13100 x 327,1; Verwendung eines charakteristischen Linienschnitts
Sensorrauschen	95% innerhalb von 46 nm PV
Kalibrierung an Tiefeneinstellnormal	7,333 µm (-2,4 %), 23,58 µm (-1,9%), 73,68 µm (-1,8%)
Geometriekorrektur	Tiefpass (1x2), Schwellwertkriterium, ungültige Pixel interpoliert und ersetzt
Datenauswertung	Geometriekorrektur über Ausgleichsgerade, λ_C-Filter 0,8 mm über NIST-Referenzsoftware (http://physics.nist.gov/VSC/jsp/FileOpen.jsp)
Hinweise	Eine eventuelle diffuse Streuung kann auch auf die Volumenstreuung des Objekts und nicht nur die Oberflächenstreuung zurückgeführt werden
Bearbeiter	Dipl. Ing. Wolfram Lyda, Dipl. Ing. David Fleischle
Ergebnisse	R_a = 0.06899 µm, R_z = 0.70701 µm W_a = 0.23 µm, W_z = 0.12799 µm

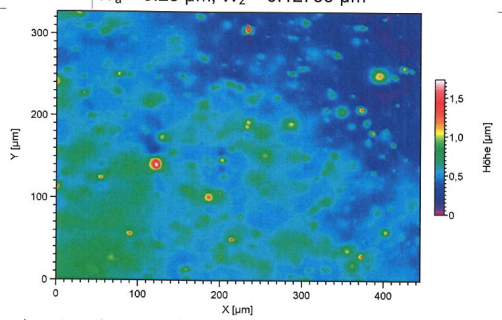

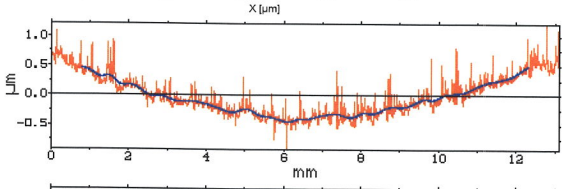

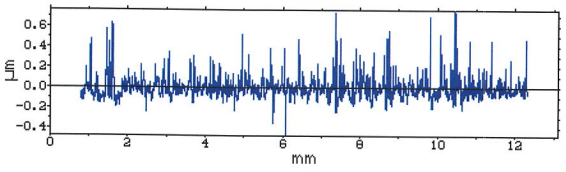

Unterschrift Sachbearbeiter

Messprotokoll

eosMetrology
TGU, TTI GmbH

Probe	Plexiglass – klare Oberfläche
Datum/Zeit	08.09.2013
Messsystem	Konfokales Mikroskop mit rotierender Mikrolinsenscheibe
Messobjektiv	50x NA 0.8 Feldgröße [µm] 444,6 x 327,1
Messbereich lateral	[µm] 13100 x 327,1; Verwendung eines charakteristischen Linienschnitts
Sensorrauschen	95% innerhalb von 37 nm PV
Kalibrierung an Tiefeneinstellnormal	7,333 µm (-2,4 %), 23,58 µm (-1,9%), 73,68 µm (-1,8%)
Geometriekorrektur	Tiefpass (1x2), Schwellwertkriterium, ungültige Pixel interpoliert und ersetzt
Datenauswertung	Geometriekorrektur über Ausgleichsgerade, λ_C-Filter 0,8 mm über NIST-Referenzsoftware (http://physics.nist.gov/VSC/jsp/FileOpen.jsp)
Hinweise	
Bearbeiter	Dipl. Ing. Wolfram Lyda, Dipl. Ing. David Fleischle
Ergebnisse	R_a = 0.00522 µm, R_z = 0.05664 µm W_a = 0.24072 µm, W_z = 0.11746 µm

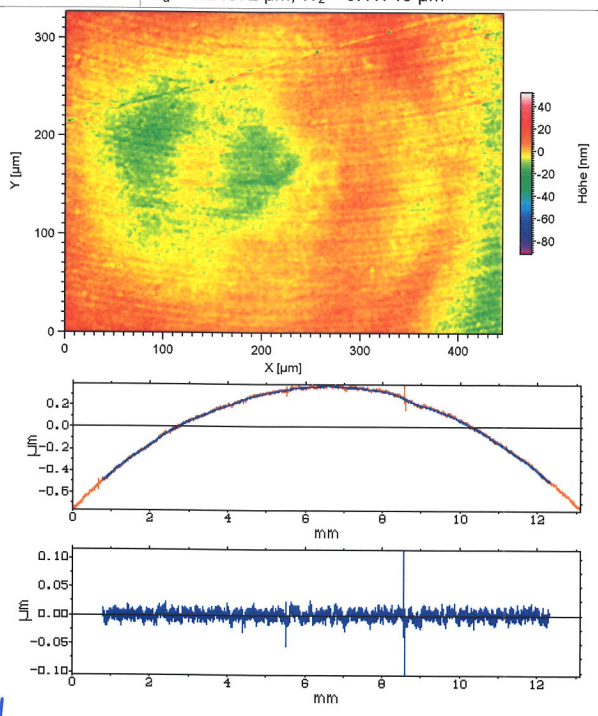

Unterschrift Sachbearbeiter

Bibliography

[1] Emissivity in the infrared theory. http://www.optotherm.com/emiss-physics.htm, 2001-2012. 9, 13

[2] Copyright ©2012. university of waikato. all rights reserved. http://www.sciencelearn.org.nz/Contexts/Light-and-Sight/Sci-Media/Images/Types-of-reflection, 22 May 2012. Accessed: 2013-10-11. ix, 11

[3] The evolution of thermal imaging cameras. http://instrumentation.com/PDFS/EvolutionThermalImagingCameras.pdf, May 2007. Accessed: 2013-10-11. 15

[4] Bebis, G., Gyaourova, A., Singh, S., and Pavlidis, I. Face recognition by fusing thermal infrared and visible imagery. *Image and Vision Computing 24*, 7 (2006), 727–742. 19

[5] Beckmann, P., and Spizzichino, A. The scattering of electromagnetic waves from rough surfaces. *Norwood, MA, Artech House, Inc., 1987, 511 p. 1* (1987). 12

[6] Benko, H., and Wilson, A. Depthtouch: Using depth-sensing camera to enable freehand interactions on and above the interactive surface. In *Proceedings of the IEEE workshop on tabletops and interactive surfaces* (2009), vol. 8. 21

[7] Bennett, H., and Porteus, J. Relation between surface roughness and specular reflectance at normal incidence. *Journal of the Optical Society of America (1917-1983) 51* (1961), 123. 11

[8] Blasko, G., Feiner, S., and Coriand, F. Exploring interaction with a simulated wrist-worn projection display. In *Proceedings of the Ninth IEEE International Symposium on Wearable Computers* (Washington, DC, USA, 2005), ISWC '05, IEEE Computer Society, pp. 2–9. 21

[9] Cao, X., and Balakrishnan, R. Interacting with dynamically defined information spaces using a handheld projector and a pen. In *Proceedings of the 19th annual ACM symposium on User interface software and technology* (New York, NY, USA, 2006), UIST '06, ACM, pp. 225–234. 21

[10] Cao, X., Forlines, C., and Balakrishnan, R. Multi-user interaction using handheld projectors. In *Proceedings of the 20th annual ACM symposium on User interface software and technology* (New York, NY, USA, 2007), UIST '07, ACM, pp. 43–52. 21

[11] Ciaramello, F. M., and Hemami, S. S. Real-time face and hand detection for videoconferencing on a mobile device. In *Workshop on Video Processing and Quality Metrics for Consumer Electronics* (2009). 38

[12] Cohen, C. J., Beach, G., and Foulk, G. A basic hand gesture control system for pc applications. In *Applied Imagery Pattern Recognition Workshop, AIPR 2001 30th* (2001), IEEE, pp. 74–79. 20

[13] Cowan, L. G., and Li, K. A. Shadowpuppets: supporting collocated interaction with mobile projector phones using hand shadows. In *Proceedings of the SIGCHI Conference on Human Factors in Computing Systems* (New York, NY, USA, 2011), CHI '11, ACM, pp. 2707–2716. 21, 22

[14] Dijkstra, K., and van Arem, H. Computer vision: Thermal imaging and infrared. http://www.optotherm.com/emiss-physics.htm, September 2012. Accessed: 2013-10-11. ix, 11

[15] Döring, T., Sahami Shirazi, A., and Schmidt, A. Exploring gesture-based interaction techniques in multi-display environments with mobile phones and a multi-touch table. In *Proceedings of the International Conference on Advanced Visual Interfaces* (2010), ACM, pp. 419–419. 21

[16] Duda, R. O., and Hart, P. E. Use of the hough transformation to detect lines and curves in pictures. *Communications of the ACM 15*, 1 (1972), 11–15. 44

[17] Greaves, A., and Rukzio, E. Evaluation of picture browsing using a projector phone. In *Proceedings of the 10th international conference on Human computer interaction with mobile devices and services* (New York, NY, USA, 2008), MobileHCI '08, ACM, pp. 351–354. 21

[18] Greensted, A. http://www.labbookpages.co.uk/software/imgproc/otsuthreshold.html. Accessed: 2013-10-09. ix, x, 34, 35, 44

[19] Harrison, C., Benko, H., and Wilson, A. D. Omnitouch: wearable multitouch interaction everywhere. In *Proceedings of the 24th annual ACM symposium on User interface software and technology* (New York, NY, USA, 2011), UIST '11, ACM, pp. 441–450. 21

[20] Heo, J., Kong, S. G., Abidi, B. R., and Abidi, M. A. Fusion of visual and thermal signatures with eyeglass removal for robust face recognition. In *Computer Vision and Pattern Recognition Workshop, 2004. CVPRW'04. Conference on* (2004), IEEE, pp. 122–122. 19

[21] Hilliges, O., Izadi, S., Wilson, A. D., Hodges, S., Garcia-Mendoza, A., and Butz, A. Interactions in the air: adding further depth to interactive tabletops. In *Proceedings of the 22nd annual ACM symposium on User interface software and technology* (New York, NY, USA, 2009), UIST '09, ACM, pp. 139–148. 20

[22] Hürst, W., and van Wezel, C. Gesture-based interaction via finger tracking for mobile augmented reality. *Multimedia Tools and Applications 62*, 1 (2013), 233–258. 21

[23] Iwai, D., and Sato, K. Heat sensation in image creation with thermal vision. In *Proceedings of the 2005 ACM SIGCHI International Conference on Advances in computer entertainment technology* (New York, NY, USA, 2005), ACE '05, ACM, pp. 213–216. 2, 20, 21

[24] Iwai, D., and Sato, K. Limpid desk: see-through access to disorderly desktop in projection-based mixed reality. In *Proceedings of the ACM symposium on Virtual reality software and technology* (2006), ACM, pp. 112–115. 2, 20

[25] Iwai, Y., Watanabe, K., Yagi, Y., and Yachida, M. Gesture recognition by using colored gloves. In *Systems, Man, and Cybernetics, 1996., IEEE International Conference on* (1996), vol. 1, pp. 76–81 vol.1. 38

[26] Izadi, S., Hodges, S., Taylor, S., Rosenfeld, D., Villar, N., Butler, A., and Westhues, J. Going beyond the display: a surface technology with an electronically switchable diffuser. In *Proceedings of the 21st annual ACM symposium on User interface software and technology* (2008), ACM, pp. 269–278. 20

[27] Kane, S. K., Avrahami, D., Wobbrock, J. O., Harrison, B., Rea, A. D., Philipose, M., and LaMarca, A. Bonfire: a nomadic system for hybrid laptop-tabletop interaction. In *Proceedings of the 22nd annual ACM symposium on User interface software and technology* (2009), ACM, pp. 129–138. 20

[28] Khan, M. M., Ingleby, M., and Ward, R. D. Automated facial expression classification and affect interpretation using infrared measurement of facial skin temperature variations. *ACM Trans. Auton. Adapt. Syst. 1*, 1 (Sept. 2006), 91–113. 18, 19

[29] Kim, D., Hilliges, O., Izadi, S., Butler, A. D., Chen, J., Oikonomidis, I., and Olivier, P. Digits: freehand 3d interactions anywhere using a wrist-worn gloveless sensor. In *Proceedings of the 25th annual ACM symposium on User interface software and technology* (2012), ACM, pp. 167–176. 61

[30] Kittel, C., and Kroemer, H. Thermal physics 2nd ed, 1980. 7, 9

[31] Koike, H., Sato, Y., and Kobayashi, Y. Integrating paper and digital information on enhanceddesk: a method for realtime finger tracking on an augmented desk system. vol. 8, pp. 307–322. 20

[32] Kong, S. G., Heo, J., Boughorbel, F., Zheng, Y., Abidi, B. R., Koschan, A., Yi, M., and Abidi, M. A. Multiscale fusion of visible and thermal ir images for illumination-invariant face recognition. *International Journal of Computer Vision 71*, 2 (2007), 215–233. 2, 19

[33] Larson, E., Cohn, G., Gupta, S., Ren, X., Harrison, B., Fox, D., and Patel, S. Heatwave: thermal imaging for surface user interaction. In *Proceedings of the SIGCHI Conference on Human Factors in Computing Systems* (New York, NY, USA, 2011), CHI '11, ACM, pp. 2565–2574. ix, 1, 2, 6, 20, 21, 24, 25

[34] Lienhart, R., and Maydt, J. An extended set of haar-like features for rapid object detection. In *Image Processing. 2002. Proceedings. 2002 International Conference on* (2002), vol. 1, IEEE, pp. I–900. 42

[35] Manresa, C., Varona, J., Mas, R., and Perales, F. Hand tracking and gesture recognition for humancomputer interaction. *Electron Letters Comput Vis Image Anal 5(3)* (2005), 96–104. 20

[36] Memarian, N., Venetsanopoulos, A. N., and Chau, T. Infrared thermography as an access pathway for individuals with severe motor impairments. *Journal of neuroengineering and rehabilitation 6*, 1 (2009), 11. 18

[37] Mistry, P., Maes, P., and Chang, L. Wuw - wear ur world: a wearable gestural interface. In *CHI '09 Extended Abstracts on Human Factors in Computing Systems* (New York, NY, USA, 2009), CHI EA '09, ACM, pp. 4111–4116. 21

[38] Murugappan, S., Vinayak, Elmqvist, N., and Ramani, K. Extended multitouch: recovering touch posture and differentiating users using a depth camera. In *Proceedings of the 25th annual ACM symposium on User interface software and technology* (New York, NY, USA, 2012), UIST '12, ACM, pp. 487–496. 20

[39] Nusca, A. Bmw night vision system uses thermal imaging to spot danger, Oct. 2009. Accessed: 2013-10-09. ix, 19

[40] Optris. infrared-camera @ONLINE, Aug. 2013. Accessed: 2013-10-11. x, 48, 49, 54, 65

[41] Otsu, N. A threshold selection method from gray-level histograms. *Automatica 11*, 285-296 (1975), 23–27. 34

[42] Pavlidis, I., Levine, J., and Baukol, P. Thermal imaging for anxiety detection. In *Computer Vision Beyond the Visible Spectrum: Methods and Applications, 2000. Proceedings. IEEE Workshop on* (2000), IEEE, pp. 104–109. 17, 18

[43] Pham, Q.-C., Gond, L., Begard, J., Allezard, N., and Sayd, P. Real-time posture analysis in a crowd using thermal imaging. In *Computer Vision and Pattern Recognition, 2007. CVPR'07. IEEE Conference on* (2007), IEEE, pp. 1–8. 18

[44] Puri, C., Olson, L., Pavlidis, I., Levine, J., and Starren, J. Stresscam: non-contact measurement of users' emotional states through thermal imaging. In *CHI '05 Extended Abstracts on Human Factors in Computing Systems* (New York, NY, USA, 2005), CHI EA '05, ACM, pp. 1725–1728. 2, 19

[45] Raheja, J. L., Das, K., and Chaudhary, A. Fingertip detection: A fast method with natural hand. *arXiv preprint arXiv:1212.0134* (2012). 38

[46] Rukzio, E., Holleis, P., and Gellersen, H. Personal projectors for pervasive computing. *IEEE Pervasive Computing 11*, 2 (Apr. 2012), 30–37. 21

[47] Rusnani, A., and Norsuzila, N. Measurement and analysis of temperature rise caused by handheld mobile telephones using infrared thermal imaging. In *RF and Microwave Conference, 2008. RFM 2008. IEEE International* (2008), IEEE, pp. 268–273. 18

[48] Sahami Shirazi, A., Döring, T., Parvahan, P., Ahrens, B., and Schmidt, A. Poker surface: combining a multi-touch table and mobile

phones in interactive card games. In *Proceedings of the 11th International Conference on Human-Computer Interaction with Mobile Devices and Services* (2009), ACM, p. 73. 21

[49] Salzberg, S. L. C4. 5: Programs for machine learning by j. ross quinlan. morgan kaufmann publishers, inc., 1993. *Machine Learning 16*, 3 (1994), 235–240. 21

[50] Schmidt, D., Molyneaux, D., and Cao, X. Picontrol: using a handheld projector for direct control of physical devices through visible light. In *Proceedings of the 25th annual ACM symposium on User interface software and technology* (New York, NY, USA, 2012), UIST '12, ACM, pp. 379–388. 21

[51] Stenger, B., Thayananthan, A., Torr, P. H., and Cipolla, R. Model-based hand tracking using a hierarchical bayesian filter. *Pattern Analysis and Machine Intelligence, IEEE Transactions on 28*, 9 (2006), 1372–1384. 45

[52] Viola, P., and Jones, M. Rapid object detection using a boosted cascade of simple features. In *Computer Vision and Pattern Recognition, 2001. CVPR 2001. Proceedings of the 2001 IEEE Computer Society Conference on* (2001), vol. 1, IEEE, pp. I–511. 40, 42

[53] Vollmer, M., Henke, S., Karstädt, D., Möllmann, K., and Pinno, F. Identification and suppression of thermal reflections in infrared thermal imaging. In *Proceedings of Inframation* (2004), vol. 5, pp. 287–298. 12, 25

[54] Wang, R. Y., and Popović, J. Real-time hand-tracking with a color glove. In *ACM Transactions on Graphics (TOG)* (2009), vol. 28, ACM, p. 63. 38

[55] Willis, K. D., Poupyrev, I., and Shiratori, T. Motionbeam: a metaphor for character interaction with handheld projectors. In *Proceedings of the SIGCHI Conference on Human Factors in Computing Systems* (New York, NY, USA, 2011), CHI '11, ACM, pp. 1031–1040. 21

[56] Wilson, A. D. Touchlight: an imaging touch screen and display for gesture-based interaction. In *Proceedings of the 6th international conference on Multimodal interfaces* (New York, NY, USA, 2004), ICMI '04, ACM, pp. 69–76. 20

[57] Wilson, A. D. Touchlight: an imaging touch screen and display for gesture-based interaction. In *Proceedings of the 6th international conference on Multimodal interfaces* (New York, NY, USA, 2004), ICMI '04, ACM, pp. 69–76. 21

[58] Wilson, A. D. Playanywhere: a compact interactive tabletop projection-vision system. In *Proceedings of the 18th annual ACM symposium on User interface software and technology* (2005), ACM, pp. 83–92. 20, 60

[59] Wilson, A. D. Depth sensing video cameras for 3d tangible tabletop interaction. In *In Proceedings of Second Annual IEEE International Workshop on Horizontal Interactive Human-Computer Systems* (2007). 20

[60] Wilson, A. D., and Benko, H. Combining multiple depth cameras and projectors for interactions on, above and between surfaces. In *Proceedings of the 23nd annual ACM symposium on User interface software and technology* (New York, NY, USA, 2010), UIST '10, ACM, pp. 273–282. 20, 21

[61] Wilson, A. D., and Benko, H. Combining multiple depth cameras and projectors for interactions on, above and between surfaces. In *Proceedings of the 23nd annual ACM symposium on User interface software and technology* (New York, NY, USA, 2010), UIST '10, ACM, pp. 273–282. 20

[62] Wilson, P. I., and Fernandez, J. Facial feature detection using haar classifiers. *Journal of Computing Sciences in Colleges 21*, 4 (2006), 127–133. x, 40

[63] Winkler, C., Pfeuffer, K., and Rukzio, E. Investigating mid-air pointing interaction for projector phones. In *Proceedings of the 2012 ACM international conference on Interactive tabletops and surfaces* (New York, NY, USA, 2012), ITS '12, ACM, pp. 85–94. 22, 59

[64] Winkler, C., Reinartz, C., Nowacka, D., and Rukzio, E. Interactive phone call: synchronous remote collaboration and projected interactive surfaces. In *Proceedings of the ACM International Conference on Interactive Tabletops and Surfaces* (New York, NY, USA, 2011), ITS '11, ACM, pp. 61–70. 21

[65] Wong, W. K., Chew, Z. Y., Loo, C. K., and Lim, W. S. An effective trespasser detection system using thermal camera. In *Computer Research and Development, 2010 Second International Conference on* (2010), IEEE, pp. 702–706. 17

[66] Wong, W. K., Lim, H. L., Loo, C. K., and Lim, W. S. Home alone faint detection surveillance system using thermal camera. In *Computer Research and Development, 2010 Second International Conference on* (2010), IEEE, pp. 747–751. 18

[67] Wong, W. K., Tan, P. N., Loo, C. K., and Lim, W. S. An effective surveillance system using thermal camera. In *Signal Acquisition and Processing, 2009. ICSAP 2009. International Conference on* (2009), IEEE, pp. 13–17. 1, 17

[68] Zivkovic, Z. Improved adaptive gaussian mixture model for background subtraction. In *Pattern Recognition, 2004. ICPR 2004. Proceedings of the 17th International Conference on* (2004), vol. 2, IEEE, pp. 28–31. 32

[69] Zivkovic, Z., and van der Heijden, F. Efficient adaptive density estimation per image pixel for the task of background subtraction. *Pattern recognition letters 27*, 7 (2006), 773–780. 32

Declaration

I hereby declare that the work presented in this thesis is entirely my own and that I did not use any other sources and references than the listed ones. I have marked all direct or indirect statements from other sources contained therein as quotations. Neither this work nor significant parts of it were part of another examination procedure. I have not published this work in whole or in part before. The electronic copy is consistent with all submitted copies.

---

place, date, signature